FINAL REPORT

NASA GRANT # NAG 8 - 636

on

THE DESIGN OF OPTICAL SENSOR FOR THE PINHOLE/OCCULTER FACILITY

by
Michael E. Greene, Ph.D.
Associate Professor

Dec 20, 1990

Table of Contents

List of Figures

I. ABSTRACT

An optical line of sight sensor system which is capable of measuring the absolute pointing angle to the sun has been designed and tested in the laboratory. The system is for use with the Pinhole\Occulter Facility, a solar hard X-ray experiment to be flown from space shuttle or space station. The sensor consists of a pinhole camera with two pairs of perpendicularly mounted linear photo diode arrays to detect the intensity distribution of the solar image produced by the pinhole, track and hold circuitry for data reduction, an analog to digital converter and a microcomputer. The deflection of the image center is calculated from these data using an approximation for the solar image. The experimental results indicate that the sensor system can estimate the image deflection within $\pm$ 2.6 μm which would correspond to $\pm$0.0167 arc seconds resolution and 0.0032 arc seconds RMS accuracy for the full scale system.

A second optical line of sight sensor system which is capable of measuring the absolute pointing angle to the sun has been designed and tested in the laboratory. The system consists of a pinhole camera with a pair of perpendicularly mounted linear photo diode arrays to detect the intensity distribution of the solar image produced by the pinhole, amplification circuitry, threshold detection circuitry and a microcomputer board. The deflection of the image is calculated by knowing the position of each pixel of the photo diode array and merely counting the pixel numbers until threshold is surpassed. From the extrapolation of laboratory data, the RMS accuracies for this system are .054 arc seconds, absolute for a 32 m P/OF.

A third optical sensor system which is capable of measuring the internal vibration of the P/OF between the mask and base has been designed, built and tested in the laboratory. The system consists of a white light source, a mirror and a pair of perpendicularly mounted linear photo diode arrays to detect the intensity distribution of the solar image produced by the mirror, amplification circuitry, threshold detection circuitry and a microcomputer board. The deflection of the image and hence the vibration of the structure is calculated by knowing the position of each pixel of the photo diode array and merely counting the pixel numbers until threshold is surpassed. From the extrapolation of laboratory data, the RMS accuracies for this system are .048 arc seconds, absolute for a 32 m structure.

II. INTRODUCTION

The Pinhole/Occulter Facility (P/OF) is a space shuttle based system for the measurement of hard X-ray and coronographic images of the sun utilizing pinhole optics for X-ray imaging. A thirty two meter flexible boom separates the mask, containing the pinholes and a corograph shield, from the detectors located in the shuttle bay. To enable reconstruction of the x-ray images [1] with spatial resolution, the mask must be pointed at the sun and the detectors aligned with the mask with a high degree of pointing accuracy and RMS stability. Knowledge of pointing accuracy is even more critical. A sketch of P/OF is shown in Figure 1.

Being a space shuttle based system, P/OF is excited by a number of disturbances which influence the pointing accuracy and stability. Chief among these are the shuttle thruster firings for orbit correction, motion induced by other systems, man motions on the shuttle, and gravity gradient torques [1-3]. A control system has been designed which uses a three axes gimbal pointing system [2, 3] to stabilize and point the system but existing sensors were determined to be inadequate for task [1].

Two sensors were determined to be required in the P/OF pointing control system. One sensor would measure the rigid body deflections of the boom/mask using a Line of Sight sensor (LOSS) while a second system would measure internal vibrations of the boom/ mask structure. A two loop controller was designed and simulated [2,3] which demonstrated the feasibility of this approach. A inner loop controller [2] stabilized the vibrational modes of the flexible boom/ mask assembly using a modal vibration sensor (MVS) and estimator. An outer loop controller used only data derived from the difference between the LOSS and the MVS to control the rigid modes of the system [3] while filtering the input to the gimbal pointing system so as not to affect the stability of the inner loop.

A LOSS which monitors the position of the mask relative to the sun center and drives a three axis gimbal system to achieve pointing of the facility has been designed previously [4,5]. This LOSS consists of a basic pinhole camera with a 5 mm pinhole built in to the facility's mask. Linear photo diode arrays were placed along perpendicular axes on the gimbal base plate 32 meters away. The arrays measure the outer edge of the solar image and a linear interpolation is used to determine the sun center. The present work reviews the main ideas behind the LOSS and the laboratory hardware used to test the

sensor as well as data indicating the accuracy of the sensor.

A second LOSS has also been designed and tested in the lab based on the LOSS built for the High Energy Imaging DevIce (HEIDi) [6,7]. This system uses a smaller pinhole along with the same linear photo diode arrays to determine sun center. The major difference is that this sensor system does not use interpolation but a simpler technique called threshold detection to determine pointing accuracy. In the present work, data from the HEIDi system is presented that is applicable to P/OF and the design changes required for adaptation to P/OF are presented also.

A modal vibration sensor (MVS) system has also been designed and tested in the lab. This system also is based on the HEIDi LOSS system. In the present work, the design is reviewed and data presented from testing the prototype system as a MVS.

Figure 1: Overview of the Pinhole/Occulter Facility

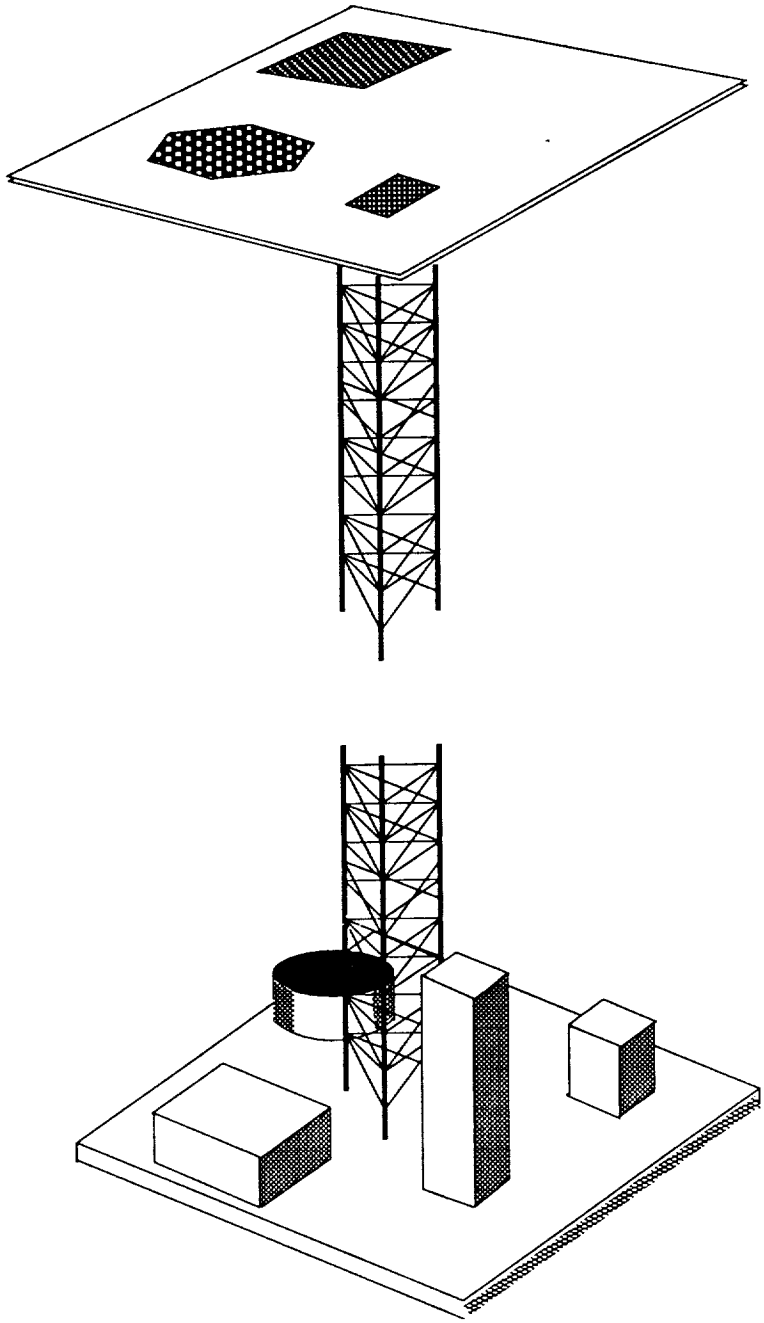

III. LINE OF SIGHT SENSOR USING IMAGE INTENSITY SLOPE DETECTION

III.A. SENSOR DESIGN

An overview of the LOSS is seen in Figure 2 where the mask containing the pinhole and base structure containing the arrays are rotated away from the sun by some angle, α. The image of the sun is deflected from (0,0) to (x_c,y_c). Arrays measure the outer edge of the solar image and output video format data. After a threshold is reached, the data from twelve diodes of each array are digitized and processed using a microcomputer, where the deflection of the solar image is calculated.

The solar image intensity distribution appears as a frustum of a cone [4] due to the smearing by the pinhole optics. In Figure 3, AA' and BB' are the linear approximation to the intensity distributions in one axis (for example X-axis) for left and right edges of the shifted solar image. AA' and BB' can expressed mathematically as

$$I_L = a(x_L + x_c) + b \tag{1}$$

and

$$I_R = -a(x_R - x_c) + b \tag{2}$$

respectively, where I is an intensity coordinate and x is a position coordinate. Solving Eqs. (1) and (2) for the sun center position, x_c, one obtains:

$$x_c = \frac{I_R - I_L}{2\,a} + \frac{x_R + x_L}{2} \tag{3}$$

Due to pixel nonuniformities, scale factor variations between arrays and noise, errors result in determination of both (x_L, I_L) and (x_R, I_R). To overcome these problems, 12 data pulses are measured for each side after the video output exceeds a set threshold. Since the 1st pixel of 12 data points can change time to time due to noise, a weighted averaging technique was used to determine both the average intensity at each pixel and the center pixel of each sample set. The weighted averages so formed then were used in Eqs (3) for (I_R, x_R) and (I_L, x_L) respectively.

Figure 2: LOSS overview using slope detection

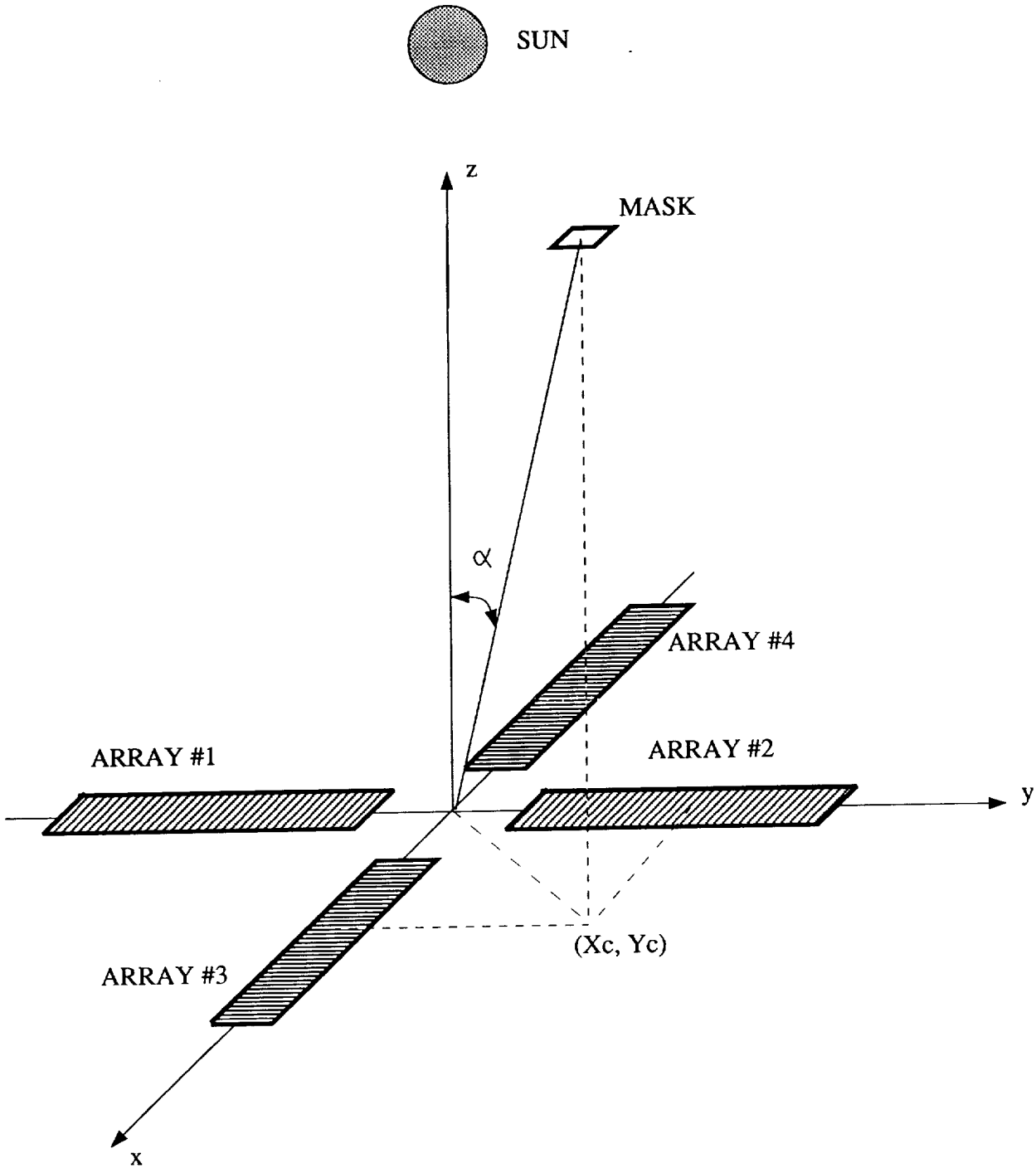

Figure 3: LOSS Algorithm Explanation

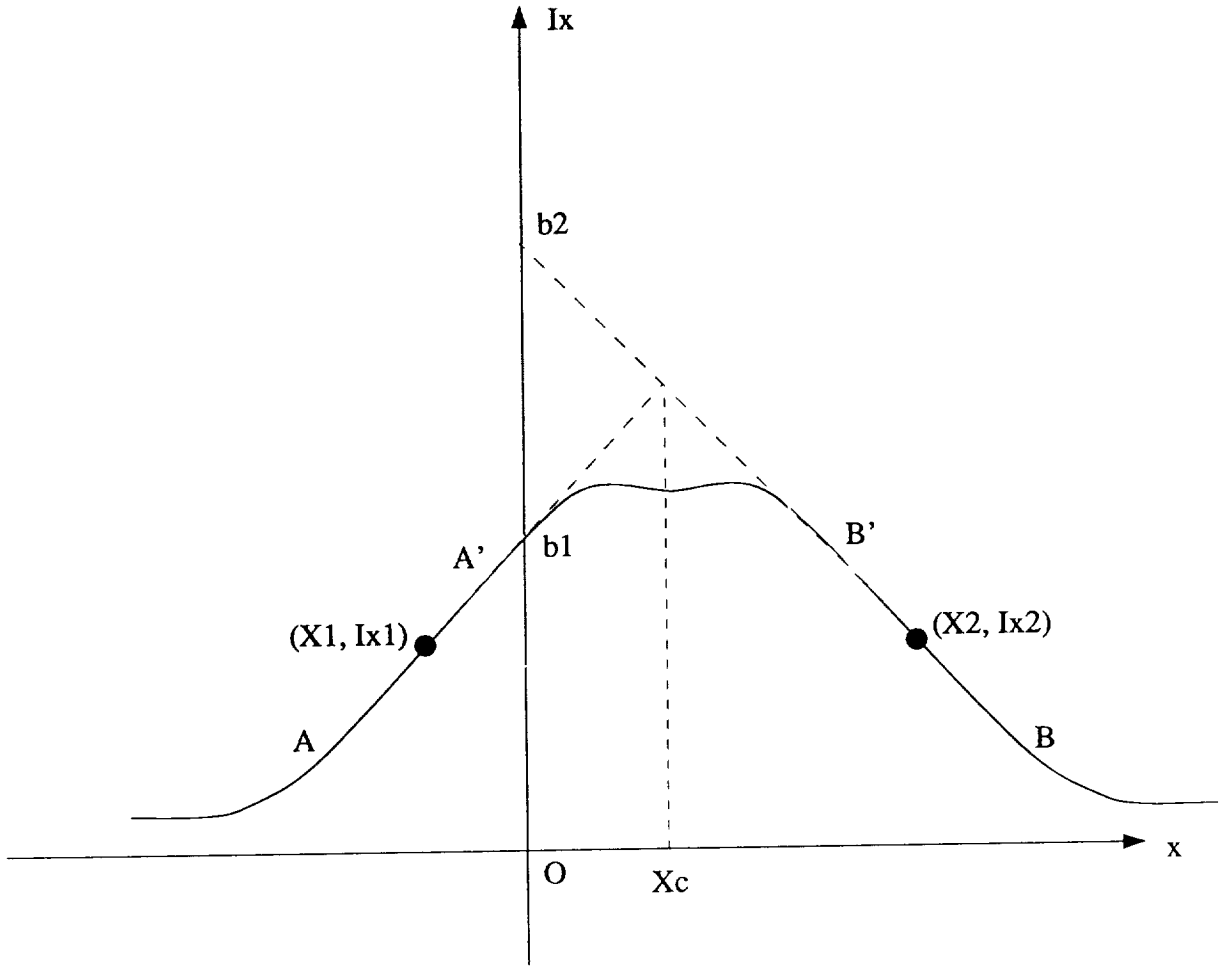

III.B. TESTING

Figure 4 is the block diagram of the LOSS hardware configuration. The arrays output the video pulse train in a preset scanning rate. Each pulse represents the light intensity received by the corresponding pixel. A start pulse must be sent before each scan of the array. This start pulse is also used as a reset of the circuits. When the video output reaches a preset threshold, 12 data pulses are sampled using the S/H circuits. Timing is controlled by the Sample and Hold controller. After 12 data have been held, a data ready pulse triggers the microcomputer to start the "Data Selector" which sends data to A/D converter. Position of the first pixel sampled is determined by counting clock pulses until the video signal reaches the threshold. The readout of the counter is then the pixel number of the first of 12 data. The counter is reset at the start of each array scan.

Calibration has been performed in one axis. Figure 5 is the laboratory setup of the experiment, mounted on a Modern Optics air optics table. A mask with 20 cm diameter cut-off and a 200 watt lamp construct the light source. Two EG&E Reticon RCO300 256X1 photo diode arrays are mounted on the stage of minimum displacement resolution of 5 μm. The center distance between two pixels of the arrays is 25 μm. Because of the limitation of the laboratory facilities' sizes, two pinholes, instead of one 5 mm pinhole, are fixed on a stage to form the same outer edge intensity functions for left and right sides as that of the real case.

An IBM PC with Model AIO8 I/O card (Industrial Computer Source) performed sampling. ICS's AIO8 is an 8 channel 12 bit high speed A/D converter with a timer/counter board. It has 4 bits digital output and 3 bits digital input. One of the 4 AIO8 counters is used as the "pixel number counter".

To test the sensor, the stage on which the arrays are mounted was displaced from a reference position. The displacements of the stage are equivalent to that of the image. The displacements were made step by step with the resolution of 5 μm and also were estimated by the sensor.

III.C. EXPERIMENTAL RESULTS

Figure 6 shows experimental mean estimation of the deflection vs. the ideal deflection. Figures 7 and 8 are the estimation mean error and standard deviation. The resolution and RMS accuracy of the line of sight sensor are

Figure 4: LOSS Hardware Block Diagram

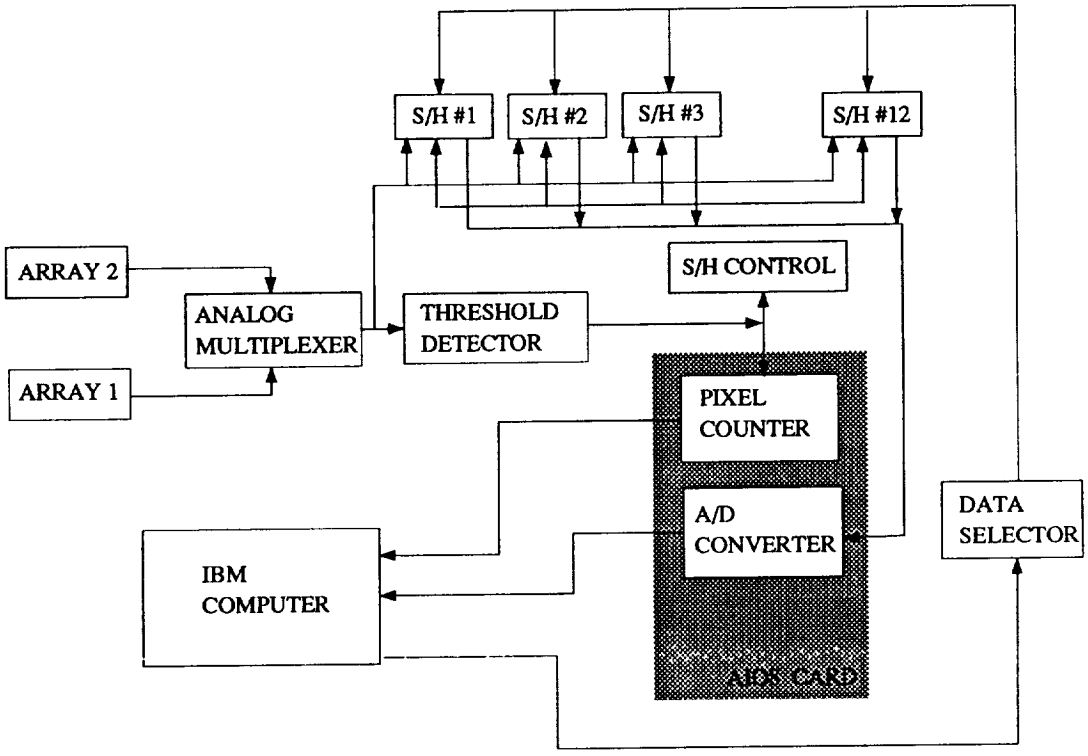

Figure 5: Laboratory Set up

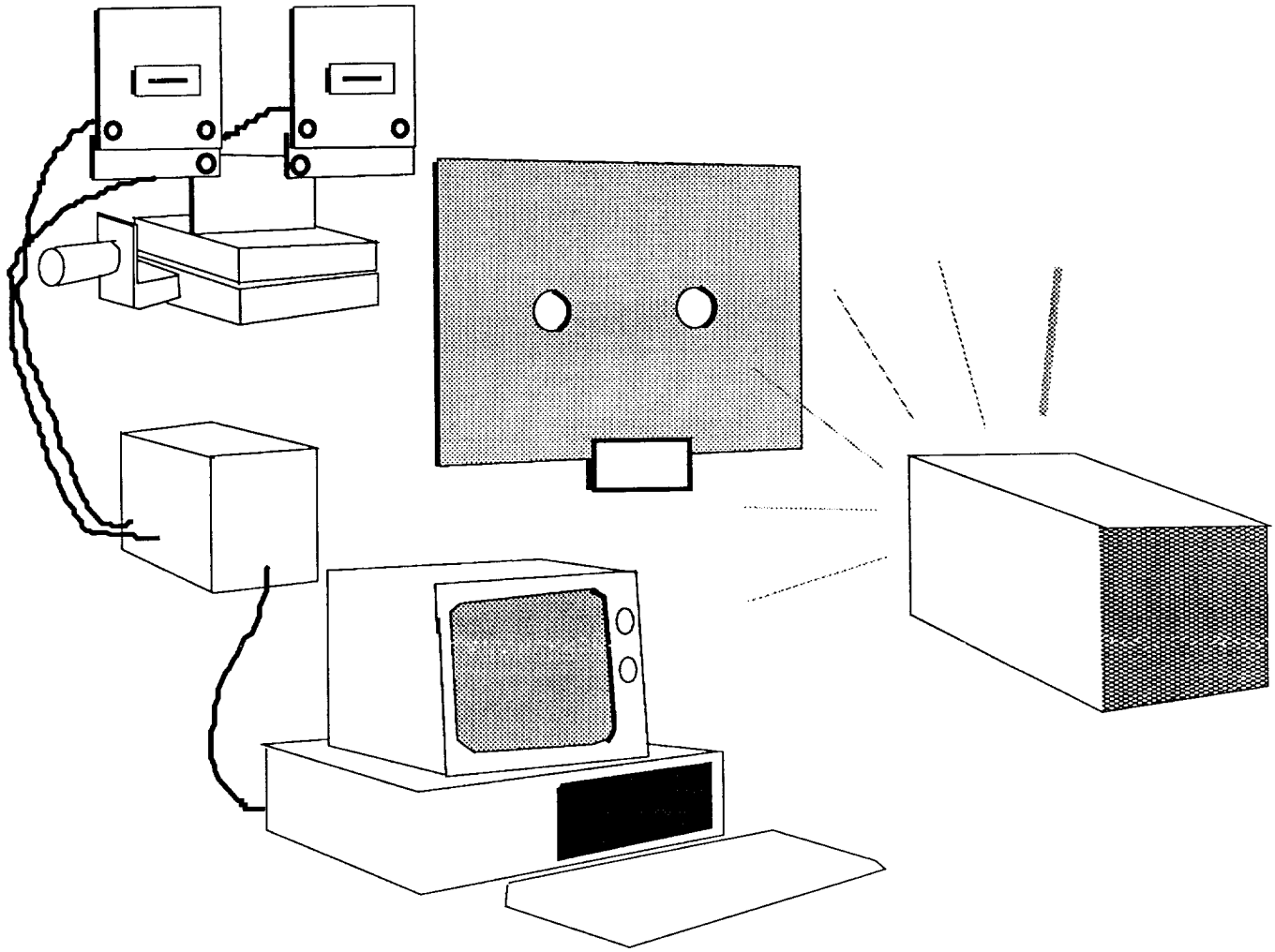

Figure 6: LOSS Estimated Position vs. Position

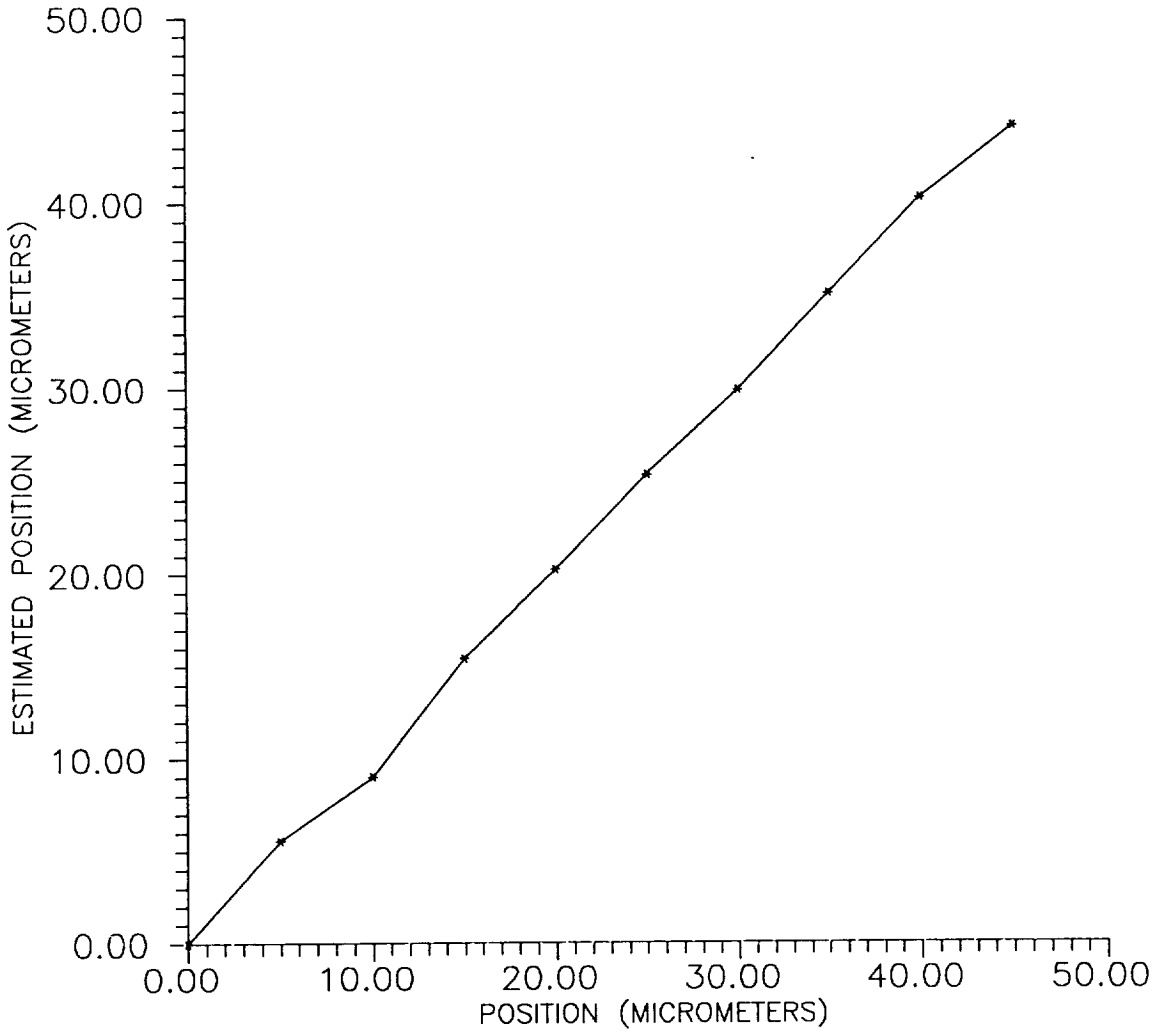

Figure 7: LOSS Mean Error in Estimate vs. Position

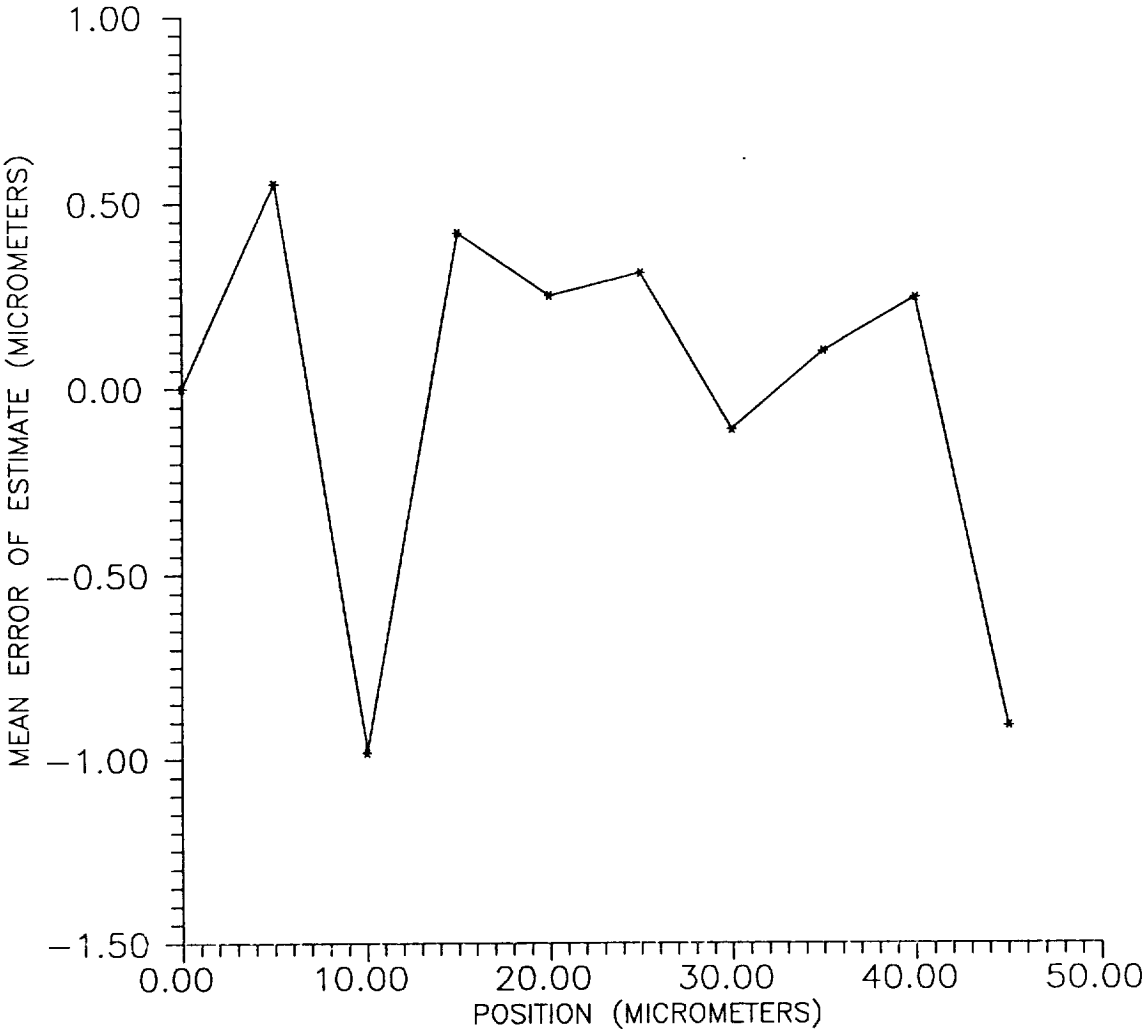

Figure 8: LOSS Standard Deviation of Estimate vs. Position

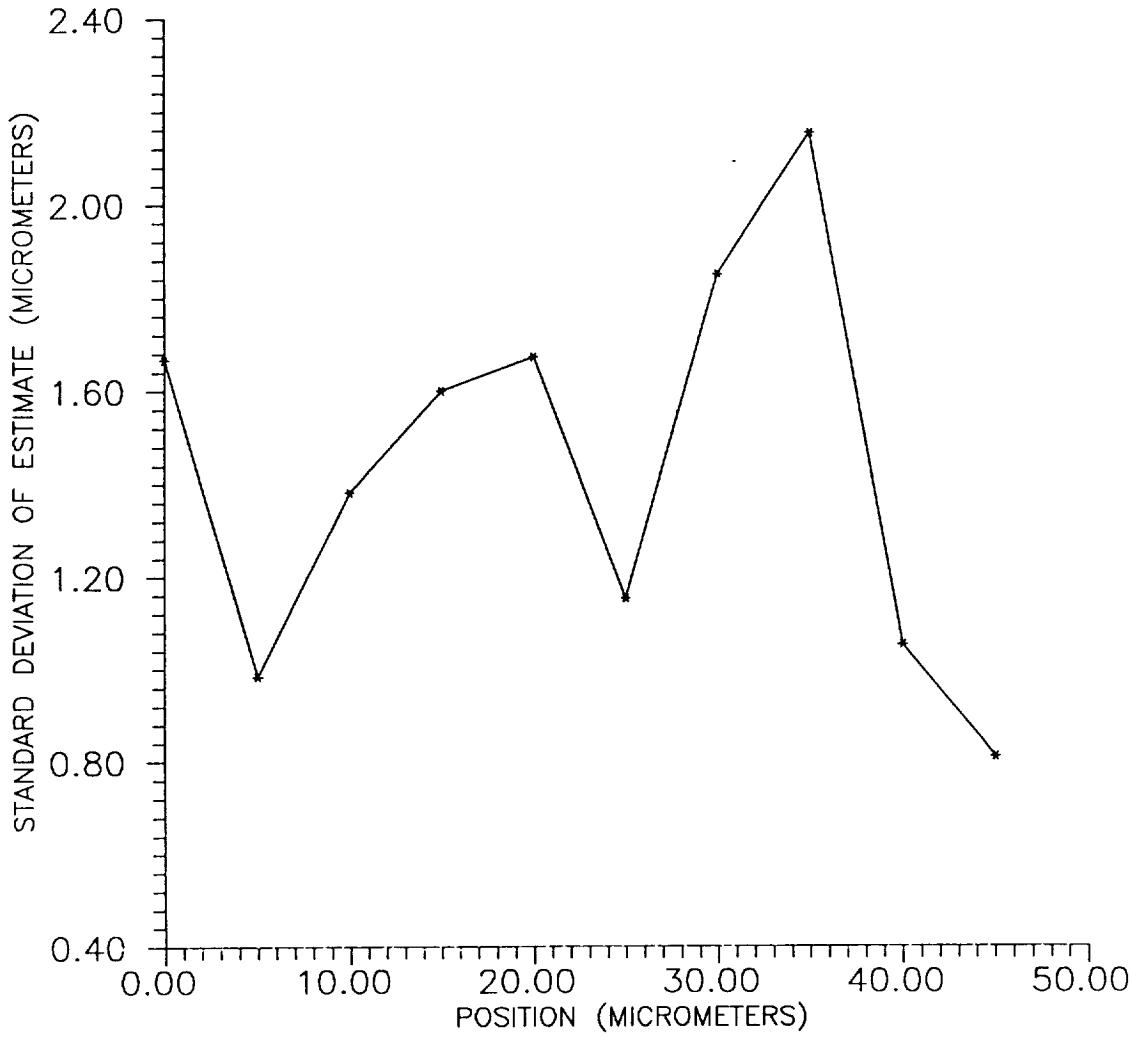

obtained as 2.5 μm and 0.5 μm respectively which translate to 0.016 arc seconds and 0.0032 arc seconds respectively in a full scale POF system.

The accuracy of testing was limited by the experimental setup and environmental noises. The mean errors fall within the experimental limits of motion control of the stage. The standard deviations of the data reflect the noise in the building more than sensor noise. The environmental noises include the building vibration, air flows in the lab room, and many other unavoidable motions.

Another source of error is uneven slopes for the left and right intensity distribution. When $\alpha_L = -\alpha_R = \alpha$, then from equation (6)

$$x_{cideal} = \left(\frac{I_R - I_L}{2\alpha} + \frac{x_L + x_R}{2}\right) \times f, \tag{7}$$

where α_L and α_R denote the left slope and right slope respectively. If $\alpha_L = \alpha + \Delta\alpha_L$ and $\alpha_R = \alpha + \Delta\alpha_R$, where $\Delta\alpha_L$ and $\Delta\alpha_R$ are small changes in slopes, then

$$x_{cpractical} = \left(\frac{I_R - I_L}{2\alpha + (\Delta\alpha_L - \Delta\alpha_R)} + \frac{\alpha(x_L + x_R) + \Delta\alpha_L x_L - \Delta\alpha_R x_R}{2\alpha + (\Delta\alpha_L - \Delta\alpha_R)}\right) \times f. \tag{8}$$

The error now can be calculated as (8) - (7):

$$\Delta x_c = \left(\frac{(I_R - I_L)(\Delta\alpha_R - \Delta\alpha_L)}{2\alpha\,(2\alpha + (\Delta\alpha_L - \Delta\alpha_R))} + \frac{(\Delta\alpha_L + \Delta\alpha_R)(x_L - x_R)}{2\,(2\alpha + (\Delta\alpha_L - \Delta\alpha_R))}\right) \times f. \tag{9}$$

The uneven slope problem could be caused by the unprecise pinhole and array alignment, sun plague, and the mask deflection in two directions which results a slight distortion of the image. Suppose α to be off ideal value by $\pm 10\%$, the magnitude of the error Δx_c from (9) is less than 0.4μm with the α and f used.

IV. LINE OF SIGHT SENSOR USING THRESHOLD DETECTION

IV.A. DESIGN

The design of the LOSS system for P/OF using threshold detection is based on the design of a similar system to be implemented on HEIDi [6,7]. HEIDi is a 5.2 m solar x-ray telescope using rotating sub collimators [8] for x-ray imaging and is to be flown on an high altitude (130,000 ft) balloon during the spring of 1992. The design goal of the aspect system or LOSS for HEIDi was .2 arc sec. RMS absolute [7]. This accuracy has been demonstrated in laboratory tests [6].

An overview of the entire pointing control system (PCS) and solar aspect system (SAS) as developed at Auburn is shown in Figure 9. The system is composed of three main subsystems: the SAS, the PCS and the sunspot detector (SPD) system. The SAS uses four photo diode arrays (PDA's) to sense the solar image, as shown in Figure 10. The array outputs are video pulses which are serially clocked out of the arrays under the control of a microcomputer unit (MCU). The pulses from each PDA are amplified and converted to an envelope by a corresponding solar limb detector card (SLD). Each SLD card signals when the video output reaches a preset threshold level and from the timing of these signal, the MCU determines on which pixel the threshold was exceeded.

Since the solar image is very sharp due to focusing by a 5.2 m lens and associated optical filtering, the change in image intensity per pixel is greater than the variability of pixel response. This results in a limitation of crossing determination to $\pm$ .5 pixel. This figure results in an RMS error of .2 arc sec in a 5.2 m telescope. In a 32 m structure, the resulting RMS accuracy would be .0325 arc sec absolute without any other design changes. The HEIDi SAS currently is capable of operating at up to 250 hz.

The difficulty with a 32 m structure, however, is that 32 m focal length lenses are not available. The use of a pinhole provides a distortion free image but the edges of the image are smeared in distance by the size of the pinhole. The pinhole can be made quite small but this drastically reduces the available light for imaging. A .1 mm pinhole is above the defraction limit but would smear the edge of the solar image over approximately .1 mm per side. The solar image changes intensity from 100% to about 20% over the same range. This results in a image intensity slope of:

$$\frac{\Delta I}{\Delta x} = \frac{100 - 20}{100} \frac{\%}{\mu m} = .8 \frac{\%}{\mu m} \tag{10}$$

Figure 9: HEIDi PCS - SAS Overview

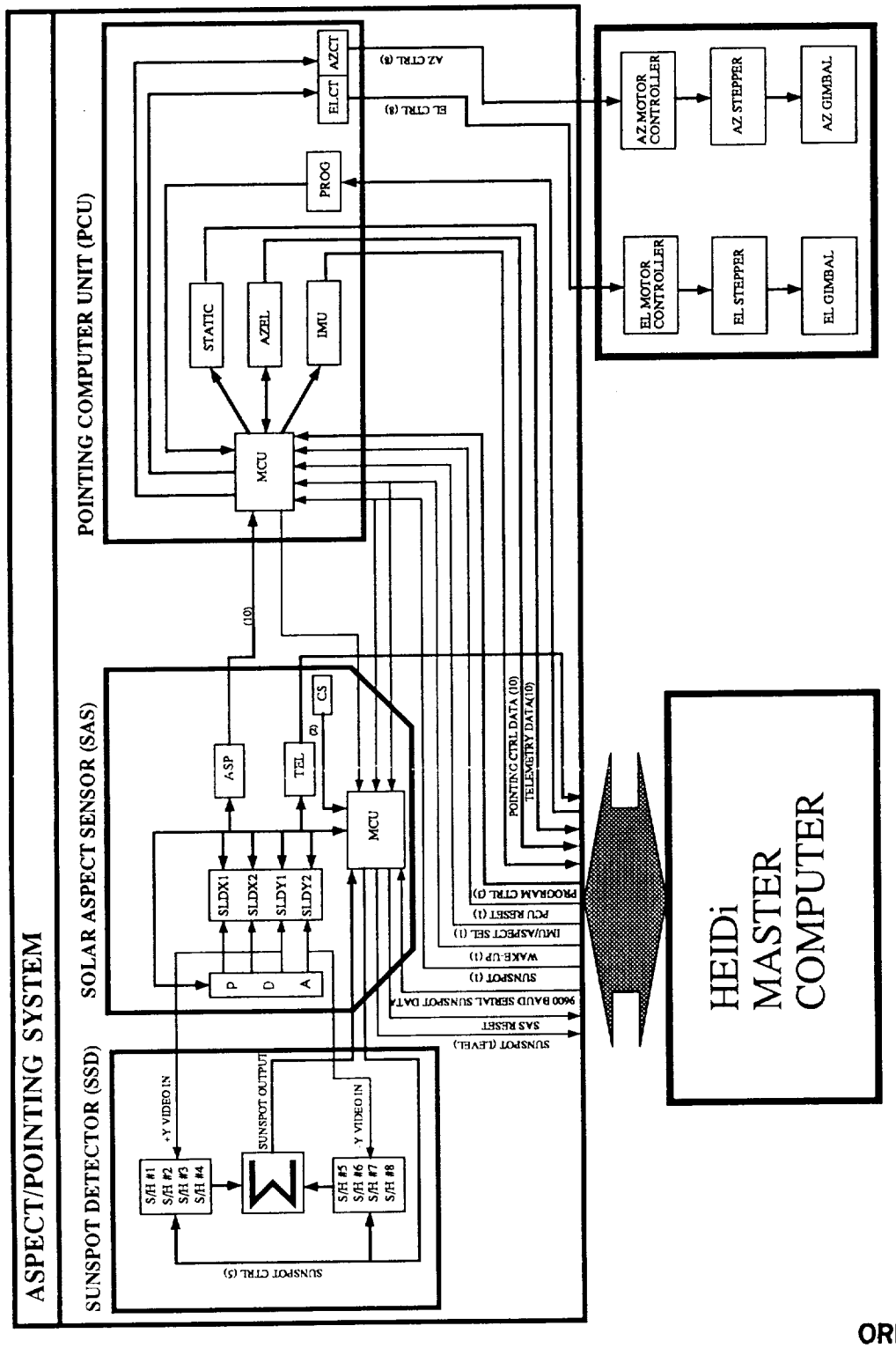

ORIGINAL PAGE IS
OF POOR QUALITY

Figure 10: HEIDi Detector

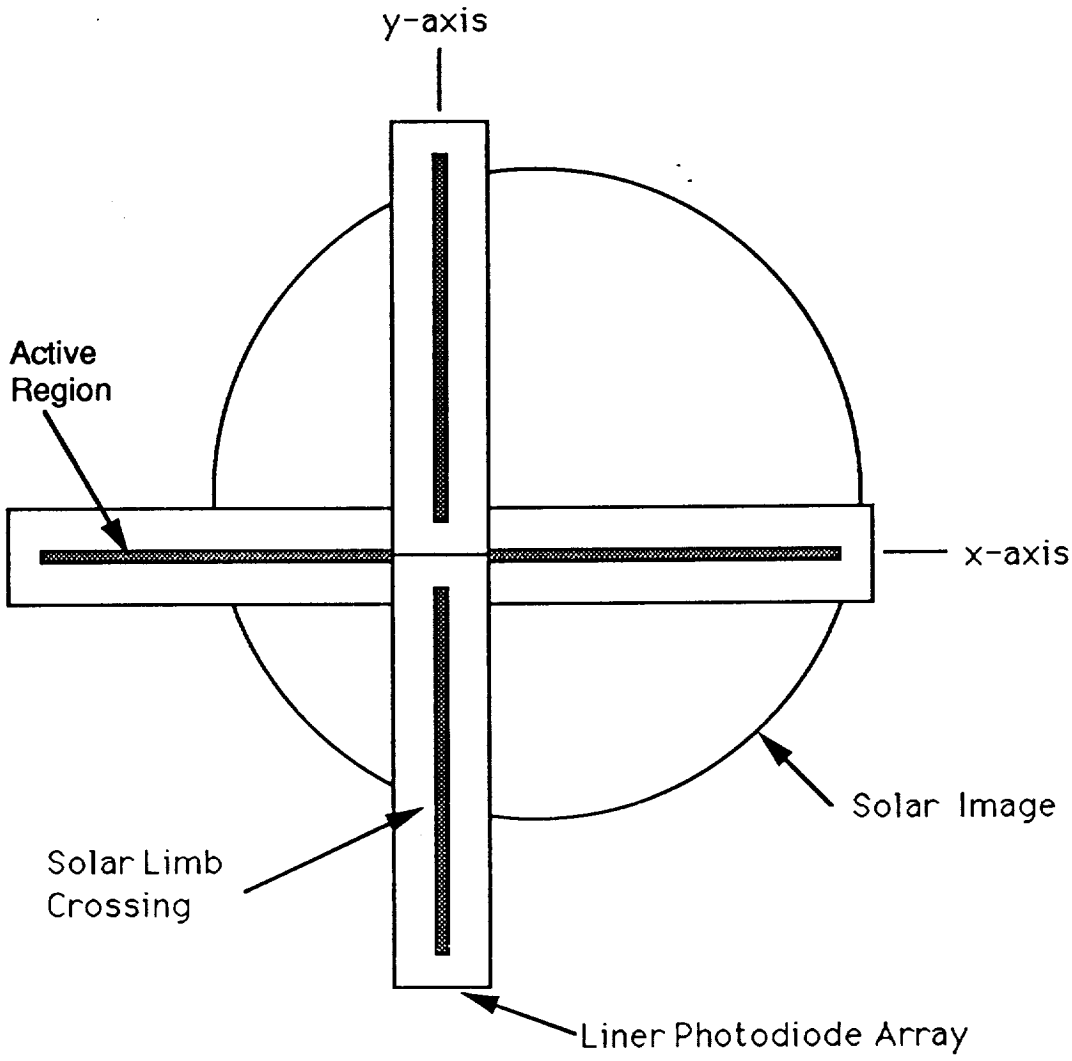

Solar Image Sensor

For the 15 μm pixels used in the HEIDi SAS, the resulting intensity change is:

$$\Delta I_{15} = .8 \times 15 = 12\ \% \tag{11}$$

which very close to the pixel nonuniformity of 10% and would necessitate the calibration and compensation of individual photo pixels. By going to 25 μm pixels the resulting intensity change would be:

$$\Delta I_{25} = .8 \times 25 = 20\ \% \tag{12}$$

which is acceptable for the threshold technique.

Similar calculations show that because of the resulting loss of intensity in the image at the detector plane with a .1 mm pinhole, a longer photo pixel integration time is required. This necessitates the slowing down of the system. The fastest rate for such a system on a 32 m structure appears to be in the 25 - 50 Hz range. Such a frequency range for the sampling period is acceptable [2] for the control of the flexible structure.

IV.B. TESTING

The solar aspect system was tested in the laboratory using the experimental setup shown in Figure 11. The solar image sensor was placed on an x - y translational stage and aligned with the output beam of the solar simulator. The optical path length of the test setup was 5.2 m. The zero positions for both the x axis and y axis were set and rechecked before taking any data. Any angle errors measured in the lab need to reduced by .2708 for the 32 m P/OF with detectors using 25 μm pixels.

The calibration of each axis was performed independently of the other with the position of the other axis set to zero for the duration of the experiment. For the x axis position of the detector arrays was varied from this initial position in 20 arc second increments (500 μm steps). At each step, one thousand data points were taken by the system and averaged. This procedure was repeated 7 times to reduce offset errors caused by improper setting of the optical stage. The same procedure was repeated for the calibration of the y axis.

Figure 11: HEIDi Laboratory Set Up

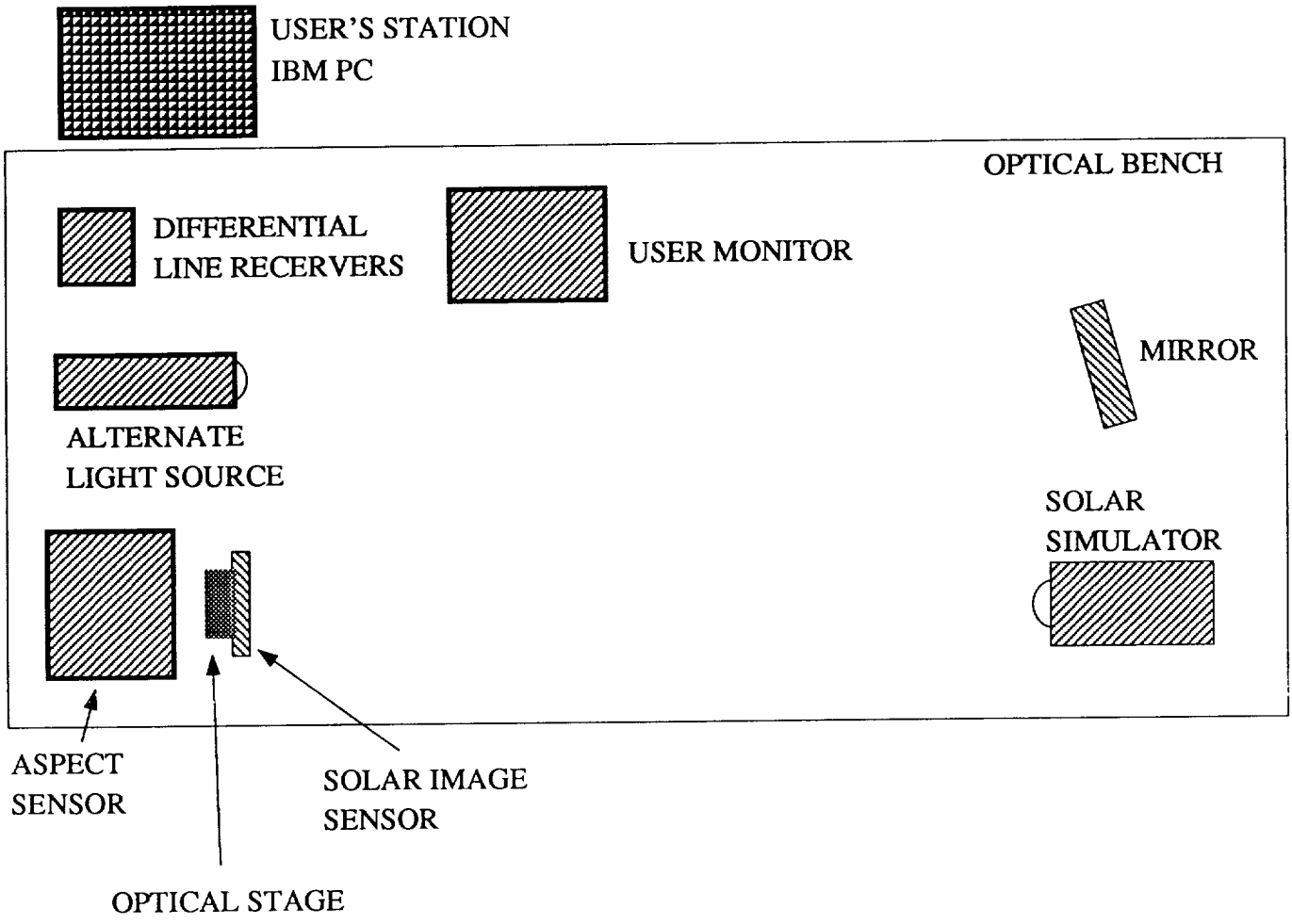

IV.C. EXPERIMENTAL RESULTS

The results of the x axis calibration are shown in Figures 12 through 19. Figure 12 shows the mean x axis error while Figure 13 shows the mean error data for each individual run. Figure 14 shows a first order approximation to data while Figure 15 show the error in the fit to the data. For a first order fit the RMS error was .12 arc sec. Figure 16 shows a second order fit to the data while Figure 17 shows the error to that fit. For a second order fit, the total RMS error was .099 arc sec. Figure 18 shows a third order fit to the data while Figure 19 shows the error to the fit. For a third order fit the total RMS error was .083 arc sec. These angles are for a 5.2 m path length.

The results of the y axis calibration are shown in Figures 20 through 27. Figure 20 shows the mean y axis error while Figure 21 shows the mean error data for each individual run. Figure 22 shows a first order approximation to data while Figure 23 show the error in the fit to the data. For a first order fit the RMS error was .42 arc sec. Figure 24 shows a second order fit to the data while Figure 25 shows the error to that fit. For a second order fit, the total RMS error was .23 arc sec. Figure 26 shows a third order fit to the data while Figure 27 shows the error to the fit. For a third order fit the total RMS error was .16 arc sec. The total RMS error for the y axis exceeded the x axis data because of a small scratch in the cover of the photo diode array at about -160 arc seconds. This scratch produces a double spike in the data as seen in Figures 20, 23, 25 and 27. In an operational system, chips with such a defect would be rejected. X axis accuracy is therefore more representative of the system. All of the above angle errors are for a 5.2 m path length.

SUMMARY OF EXPERIMENTAL RESULT (ARC SECONDS)				
	X - Axis		Y - Axis	
Compensation	5.2 m	32 m	5.2 m	32 m
None	.387	.104	.415	.112
1st Order	.120	.033	.227	.061
2nd Order	.099	.027	.210	.057
3rd Order	.083	.022	.155	.042

Note: All error figures for 32 m are based on using 25 μm photo pixels.

Figure 12: X axis Total Mean Error vs. Position

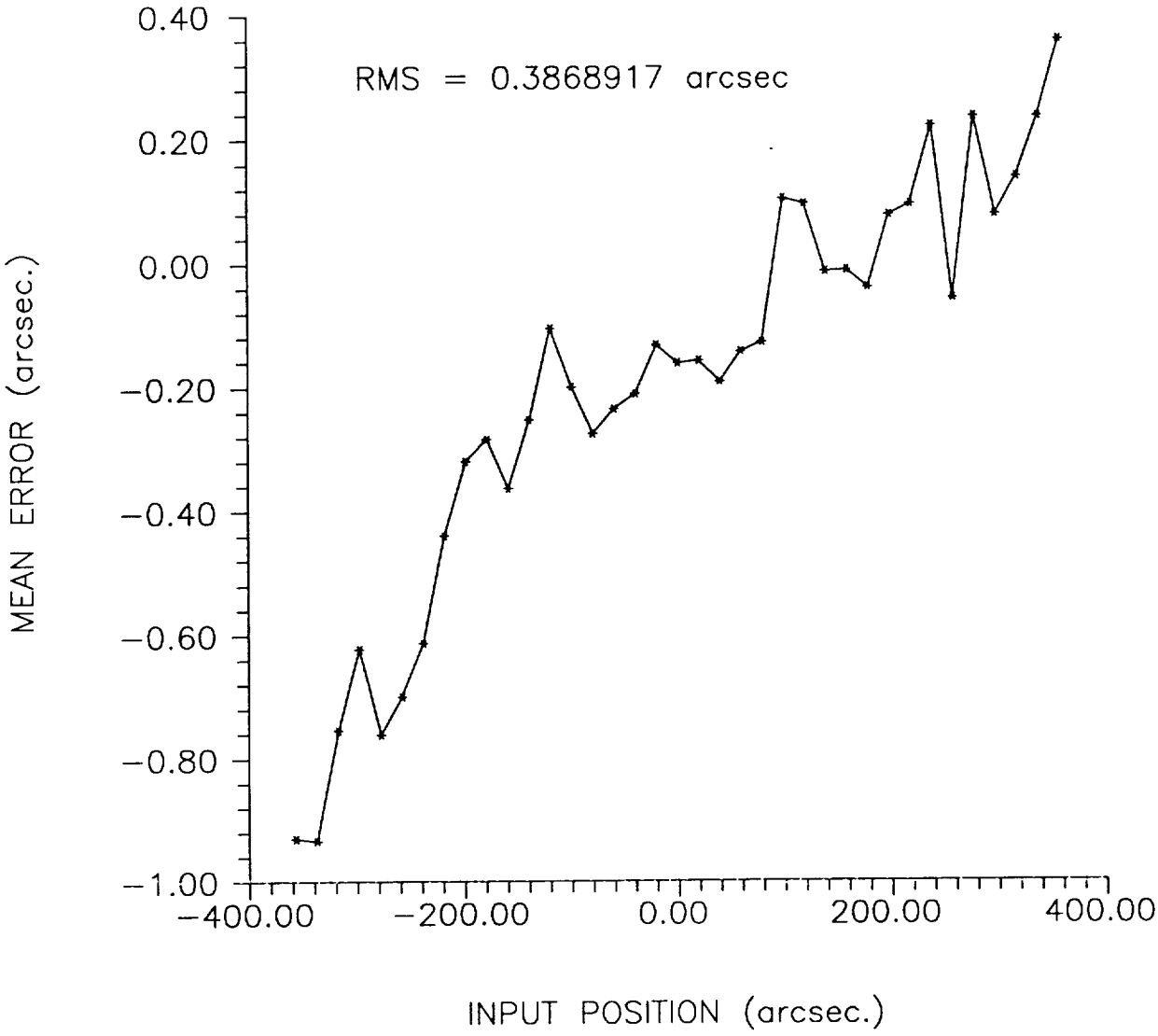

Figure 13: X axis Mean Error/Test vs. Position

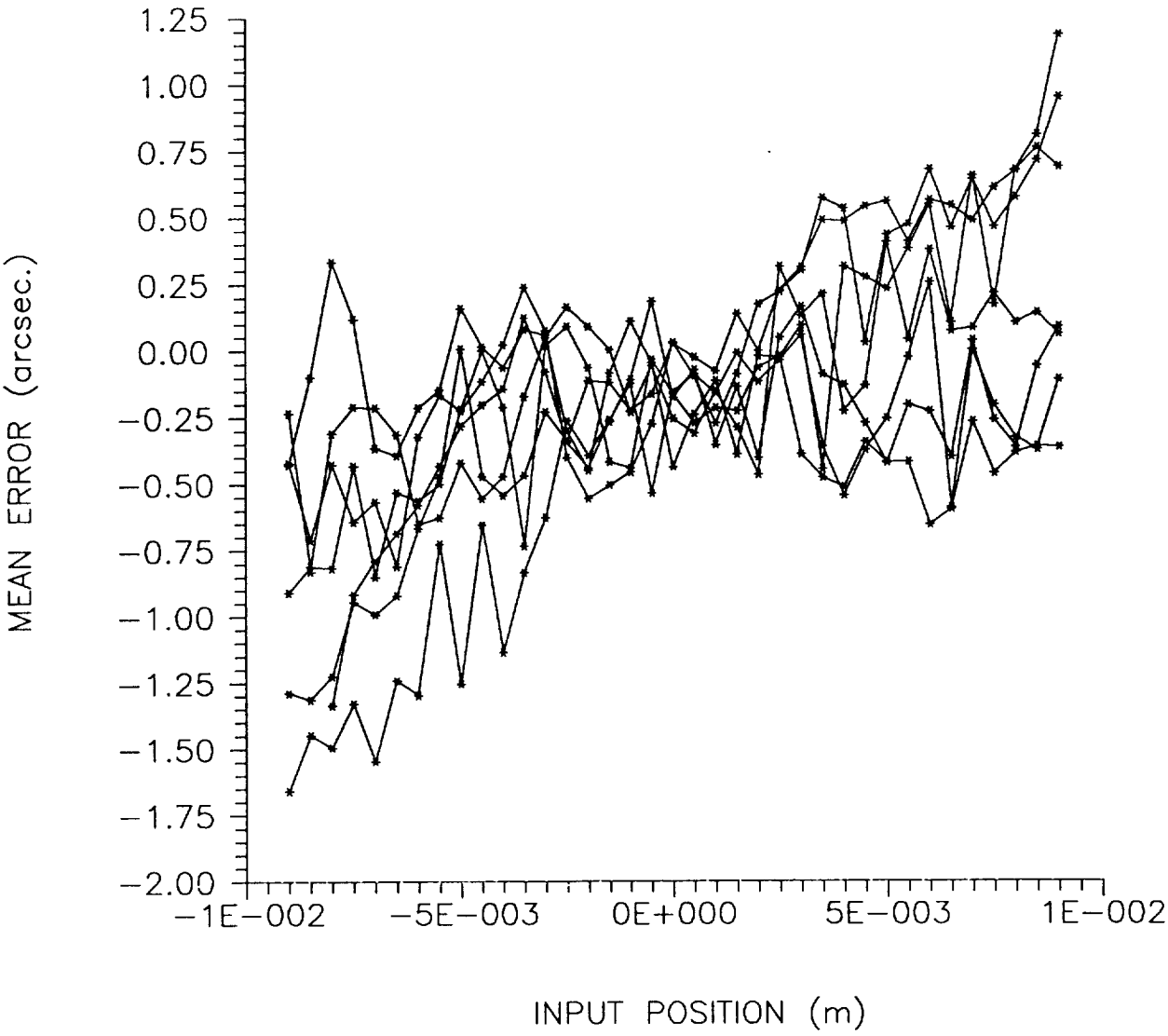

Figure 14: X axis First Order Approximation

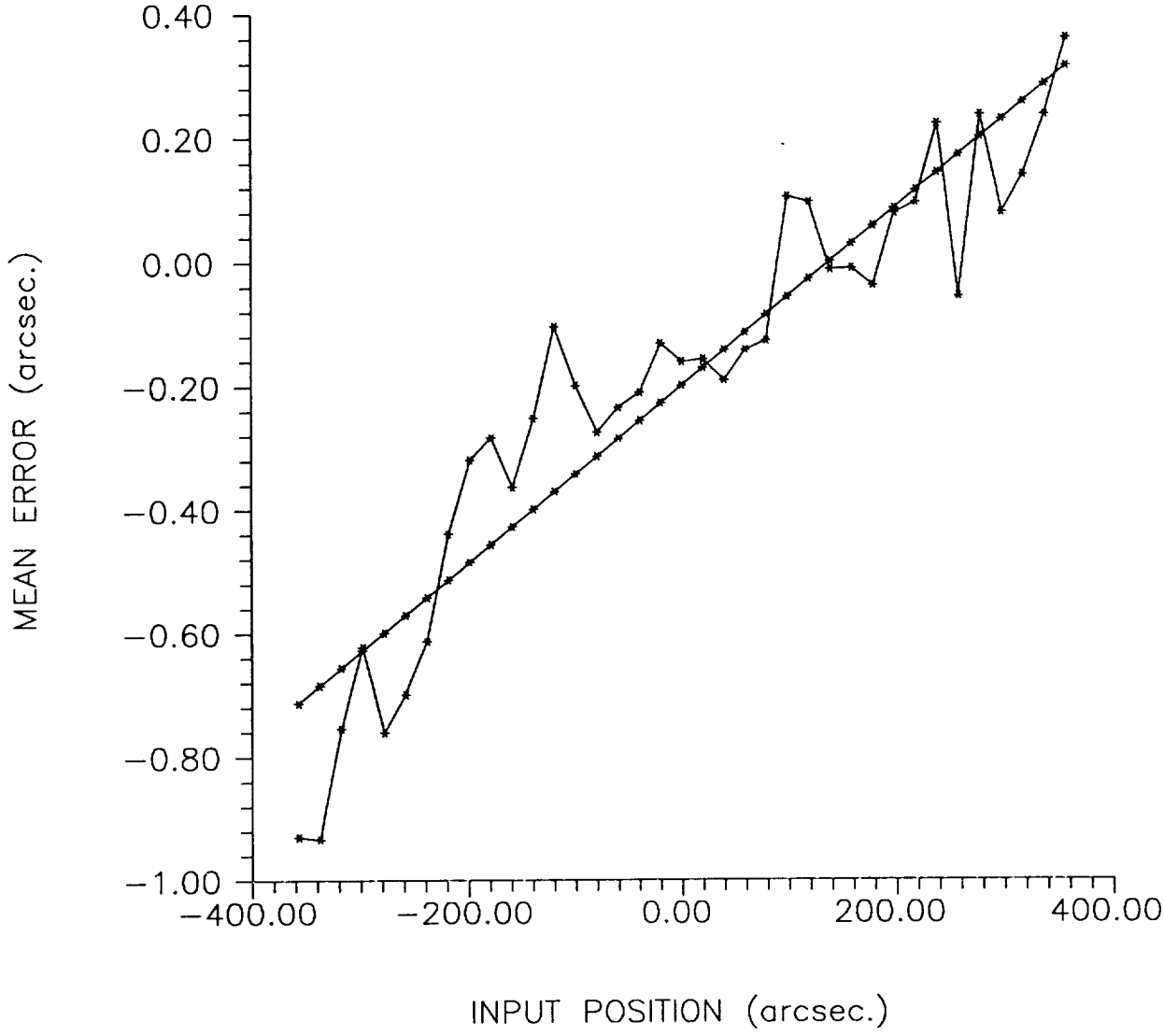

Figure 15: X axis First Order Approximation Error

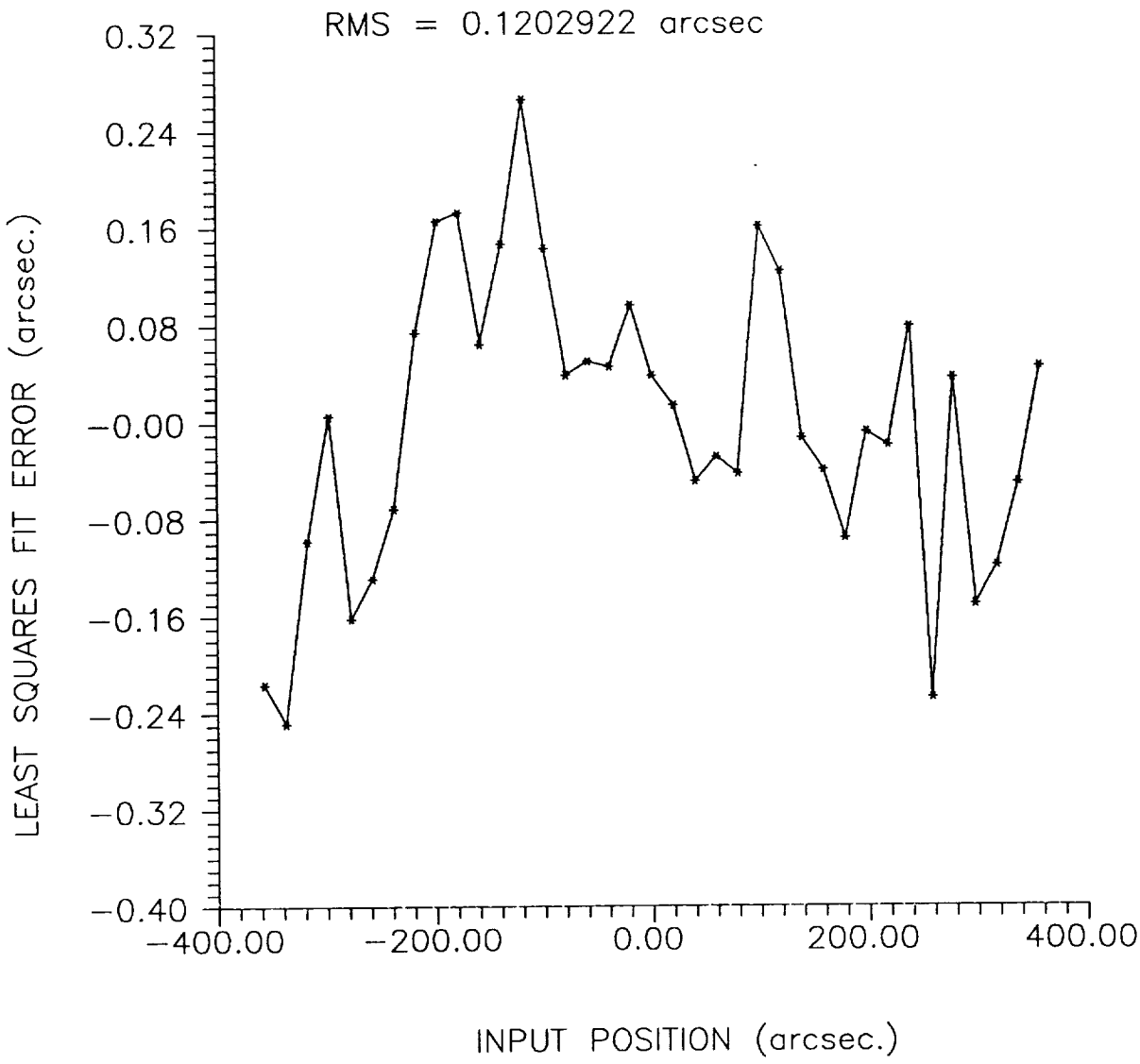

Figure 16: X axis Second Order Approximation

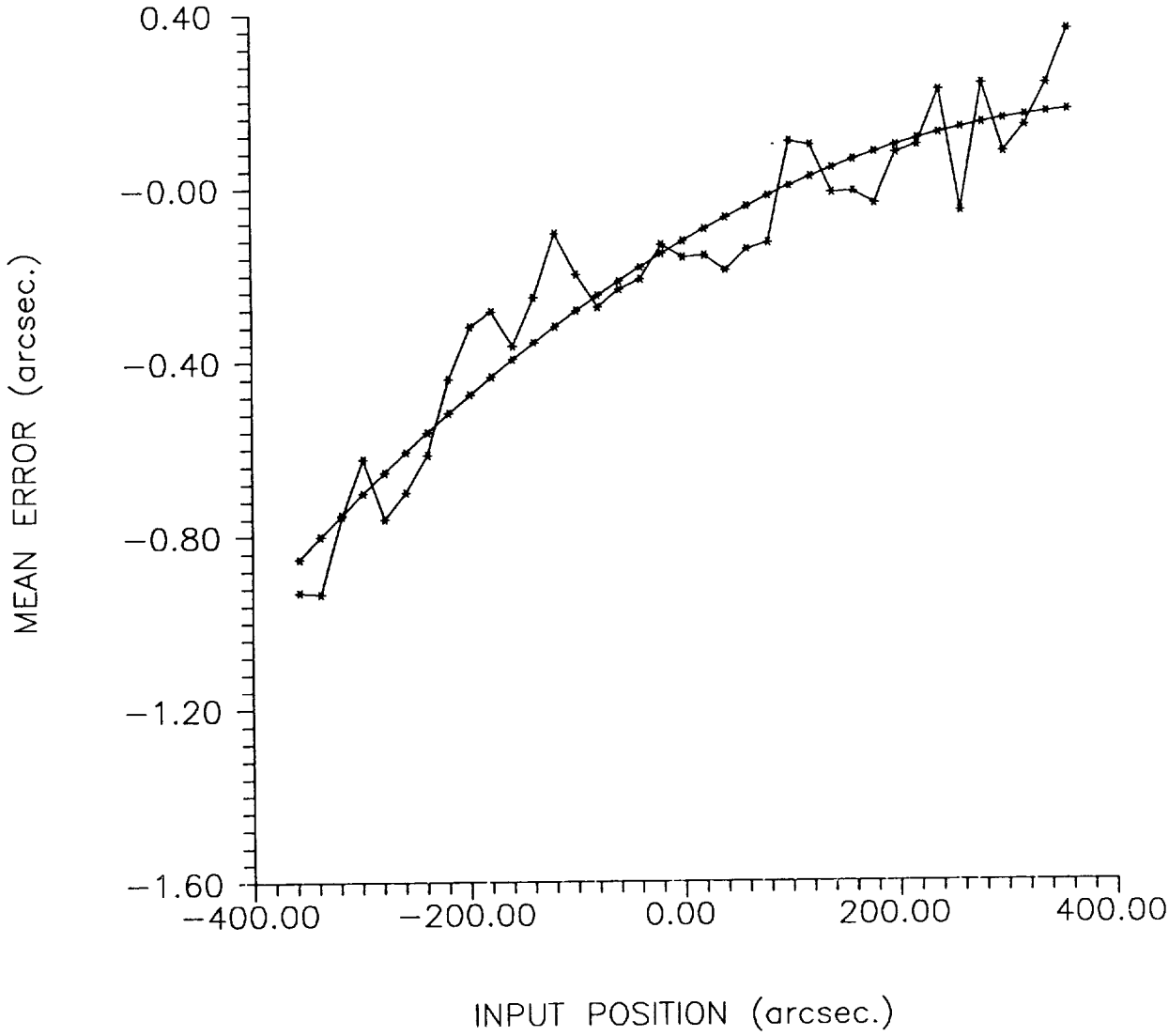

Figure 17: X axis Second Order Approximation Error

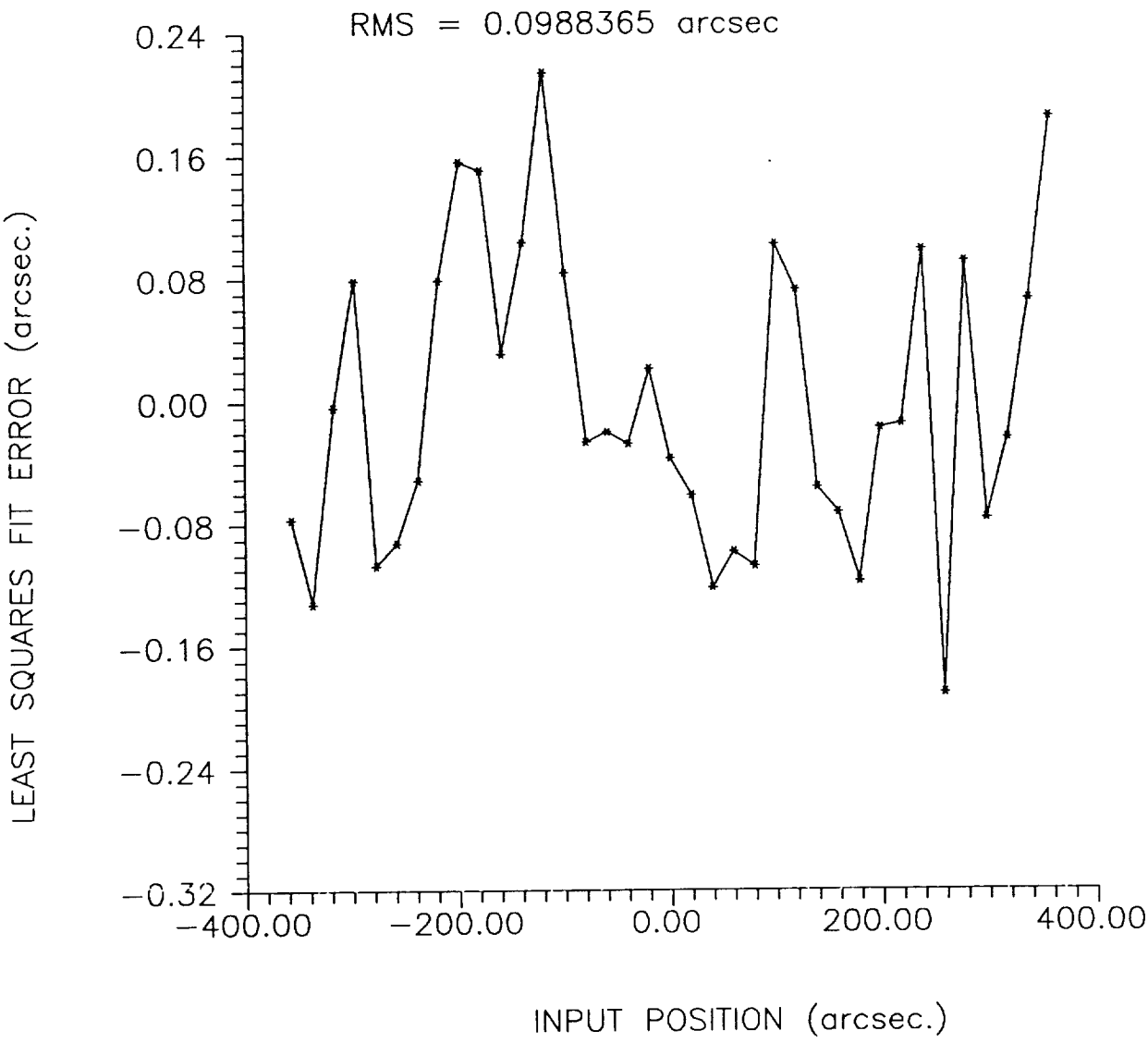

Figure 18: X axis Third Order Approximation

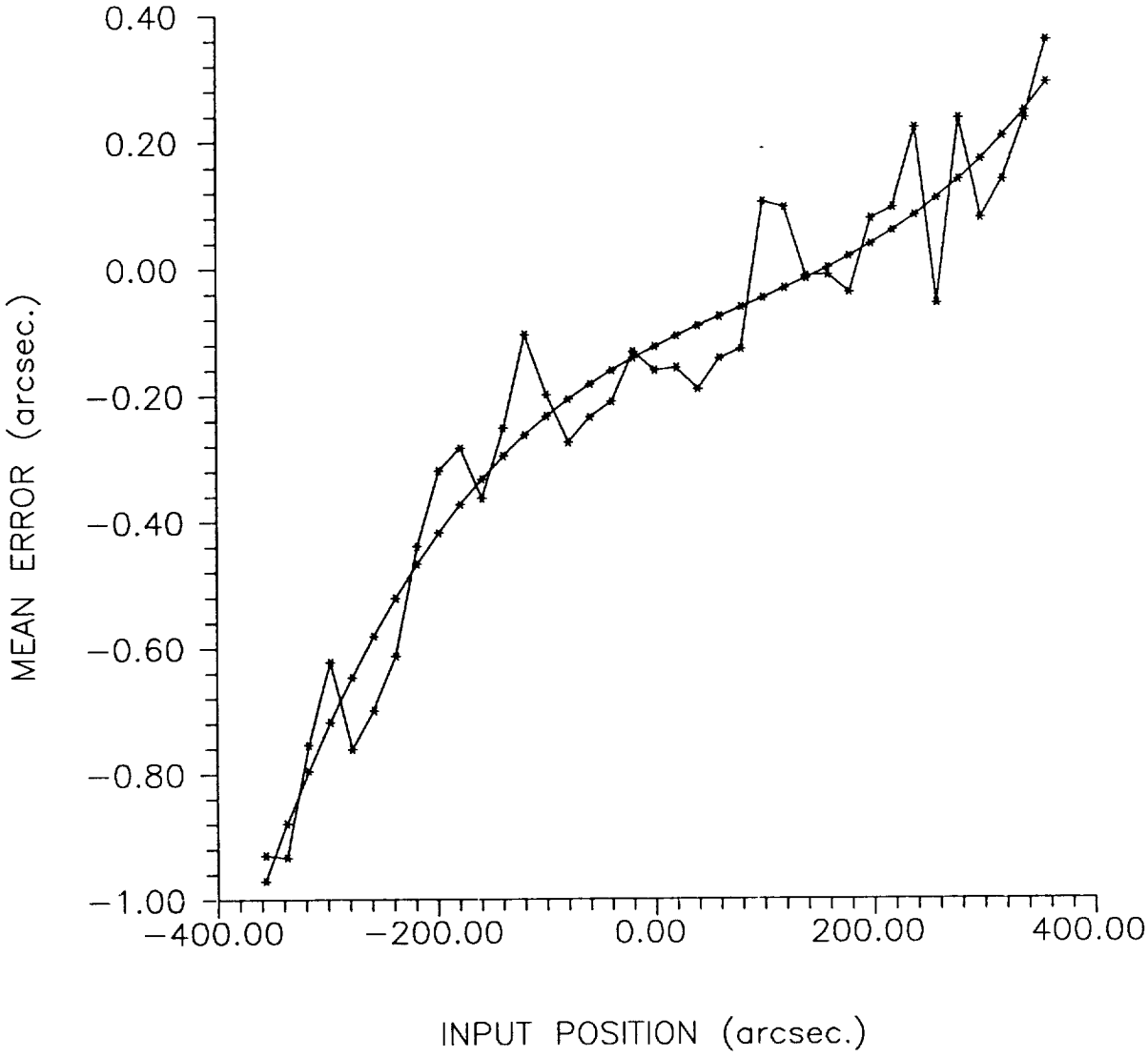

Figure 19: X axis Third Order Approximation Error

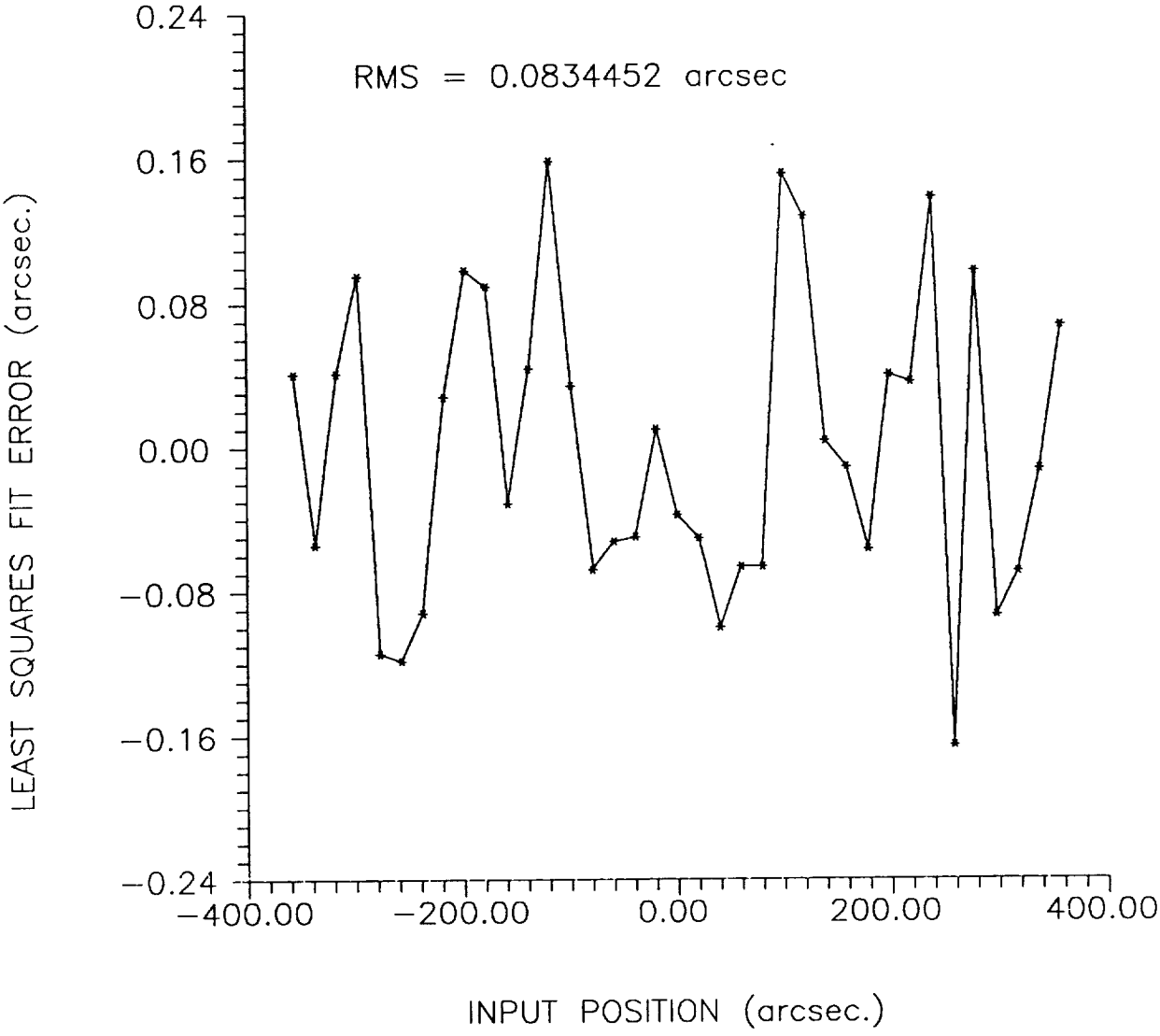

Figure 20: Y axis Total Mean Error vs. Position

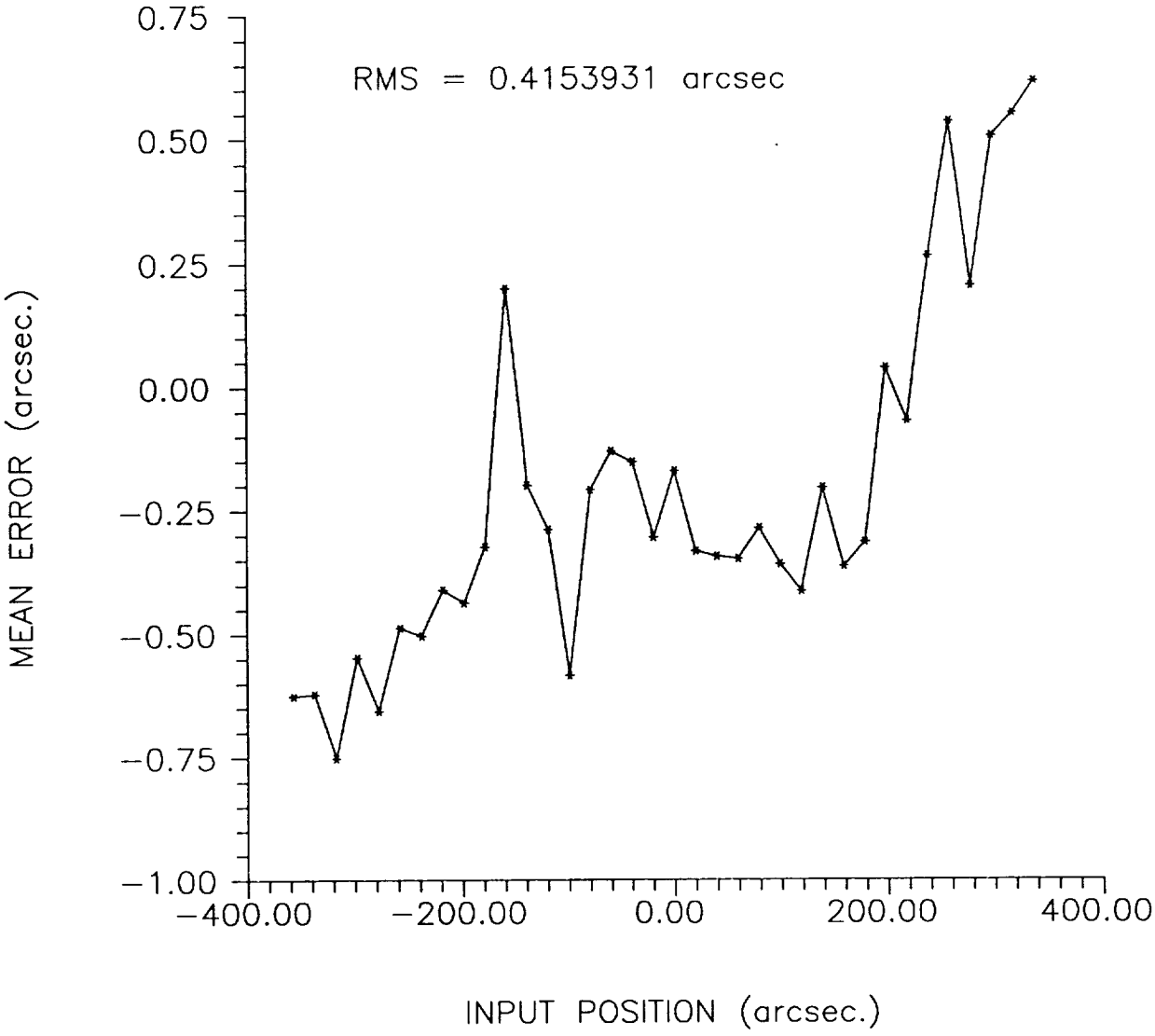

Figure 21: Y axis Mean Error/Test vs. Position

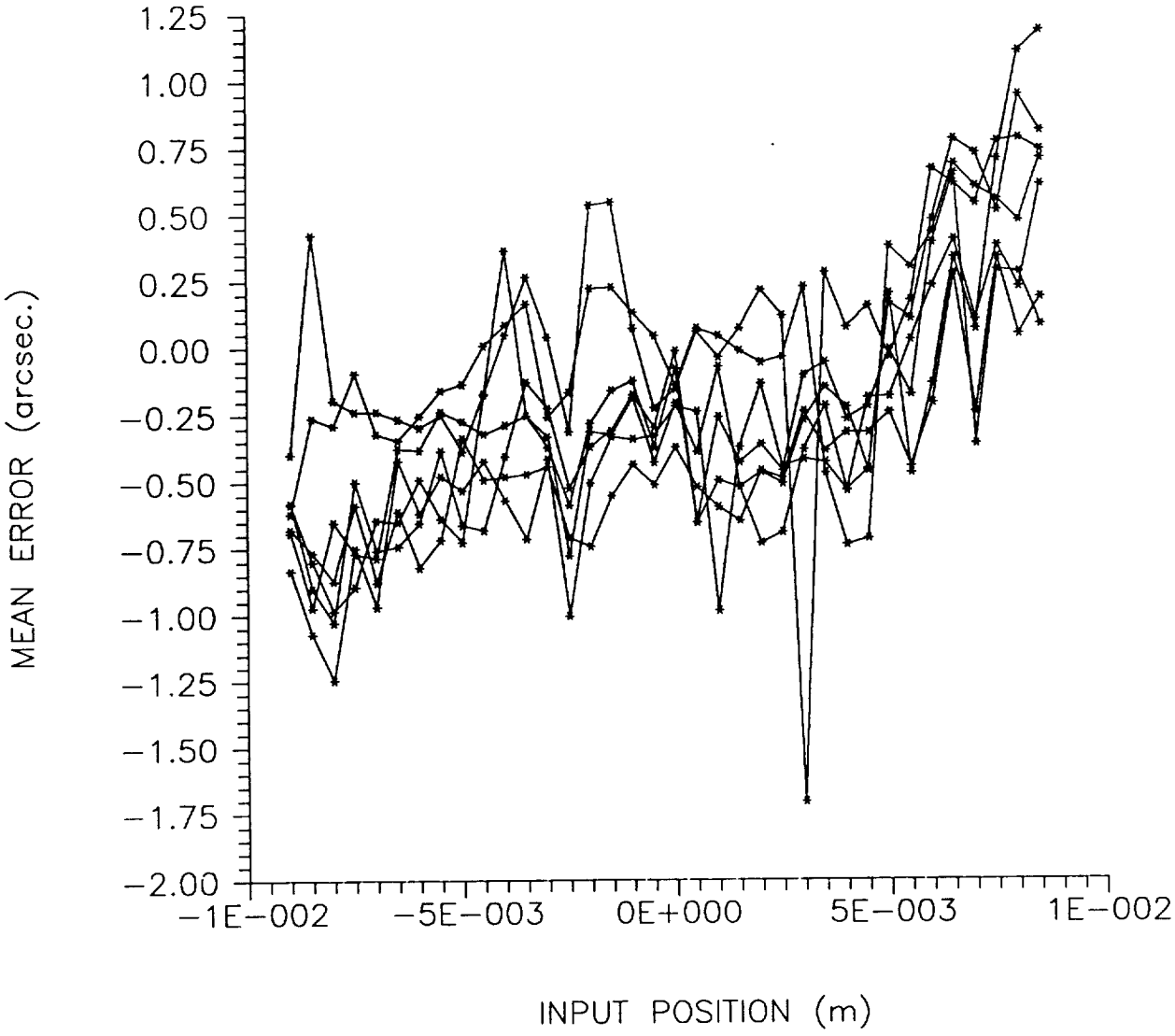

Figure 22: Y axis First Order Approximation

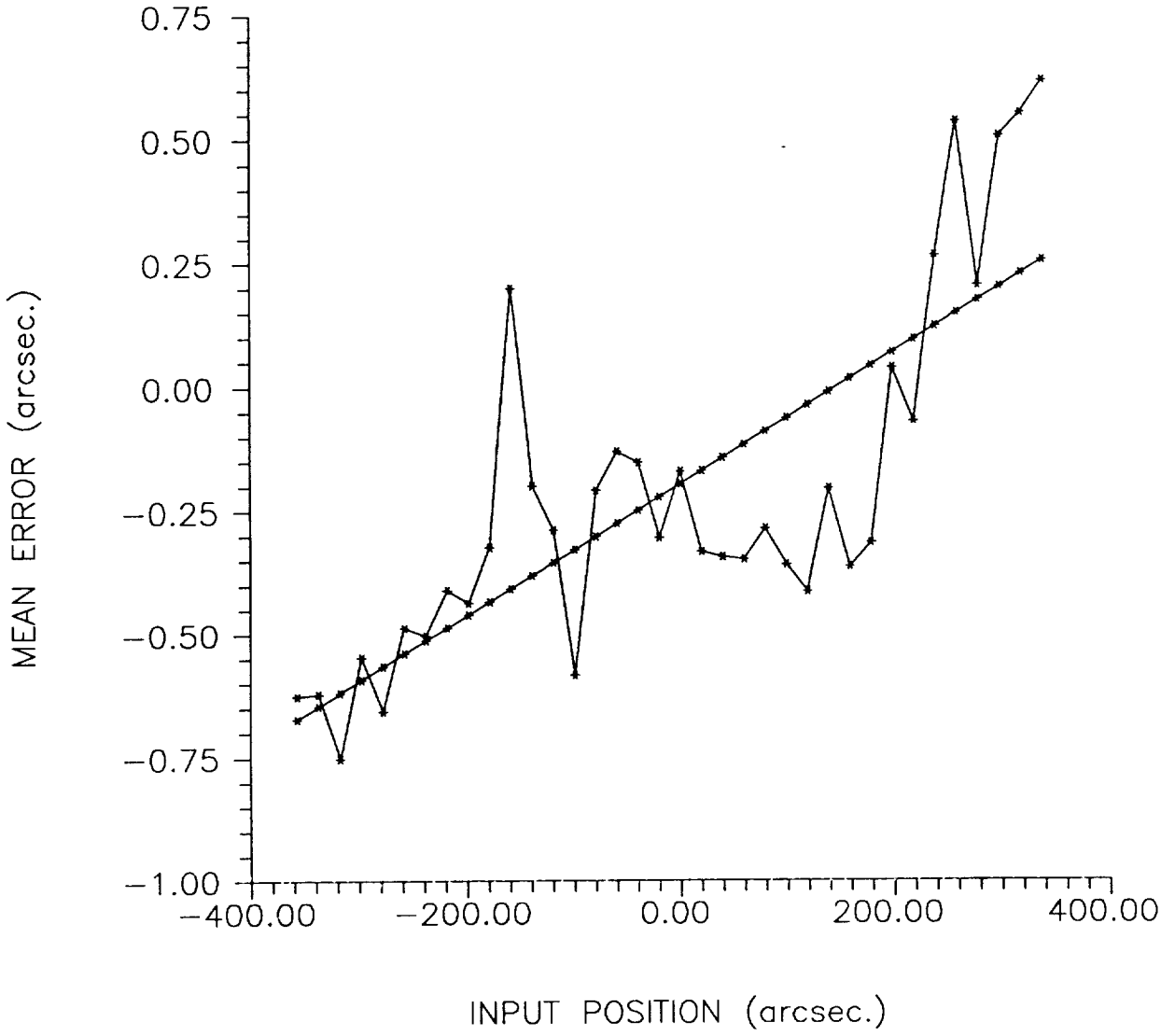

Figure 23: Y axis First Order Approximation Error

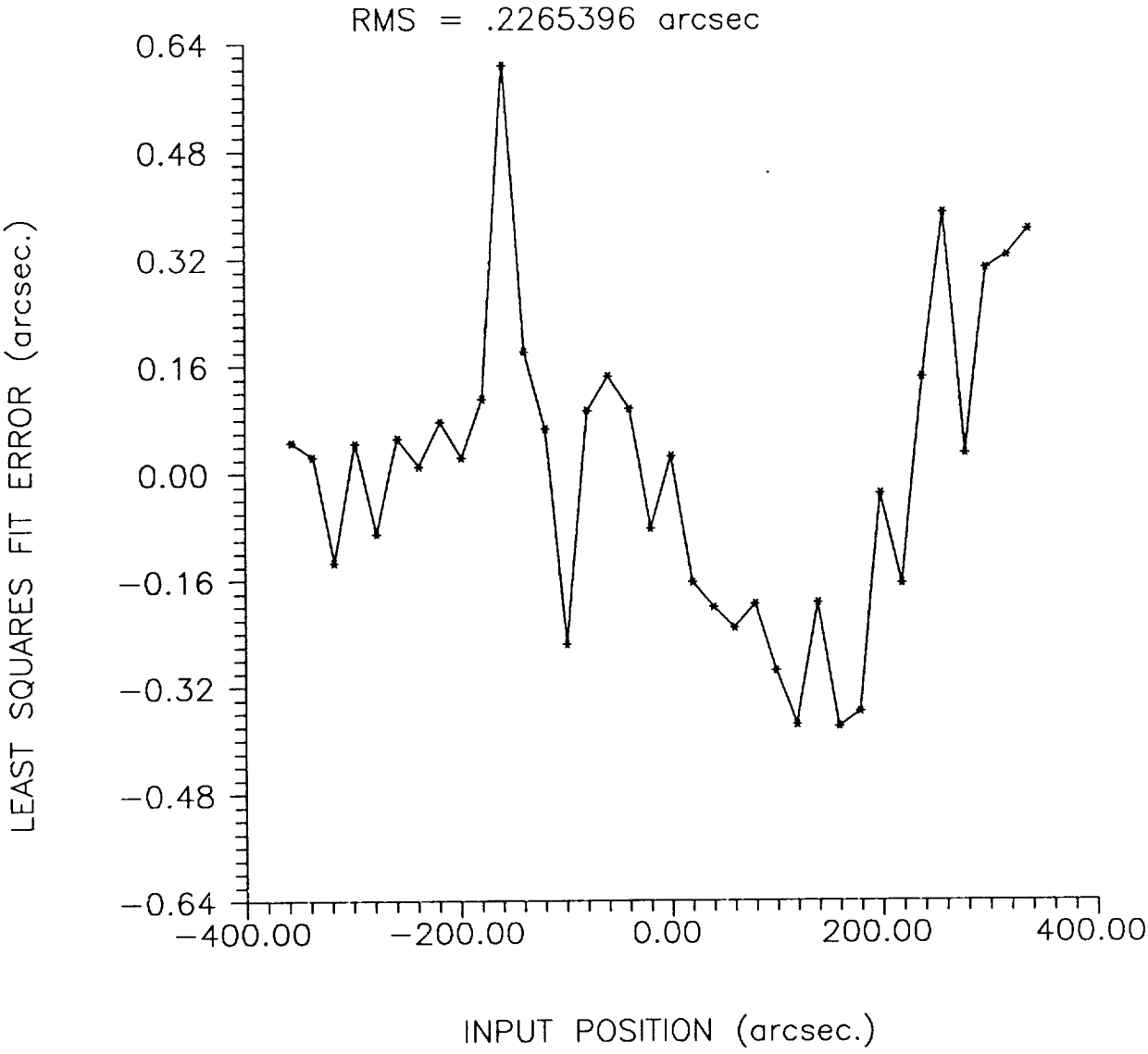

Figure 24: Y axis Second Order Approximation

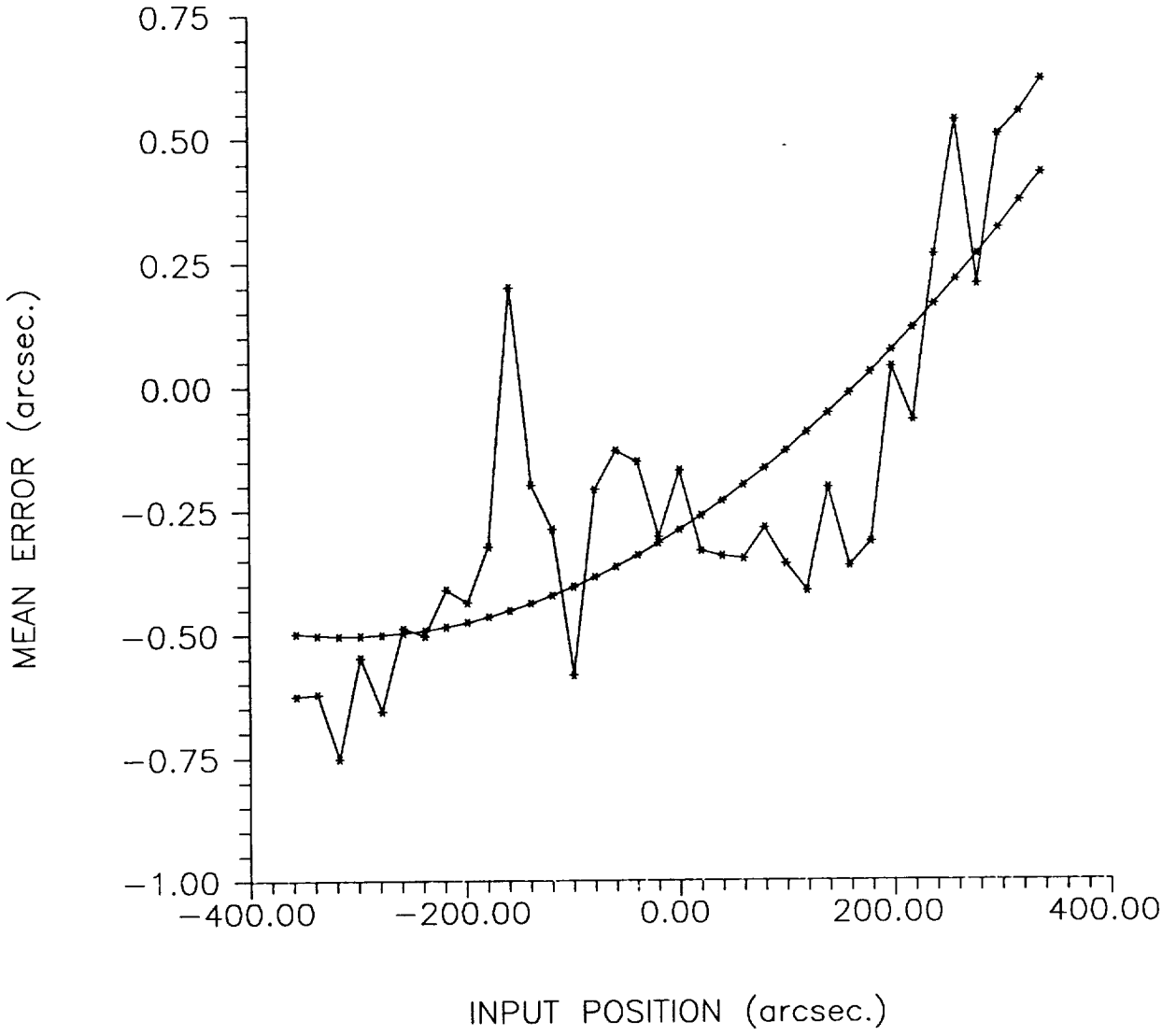

Figure 25: Y axis Second Order Approximation Error

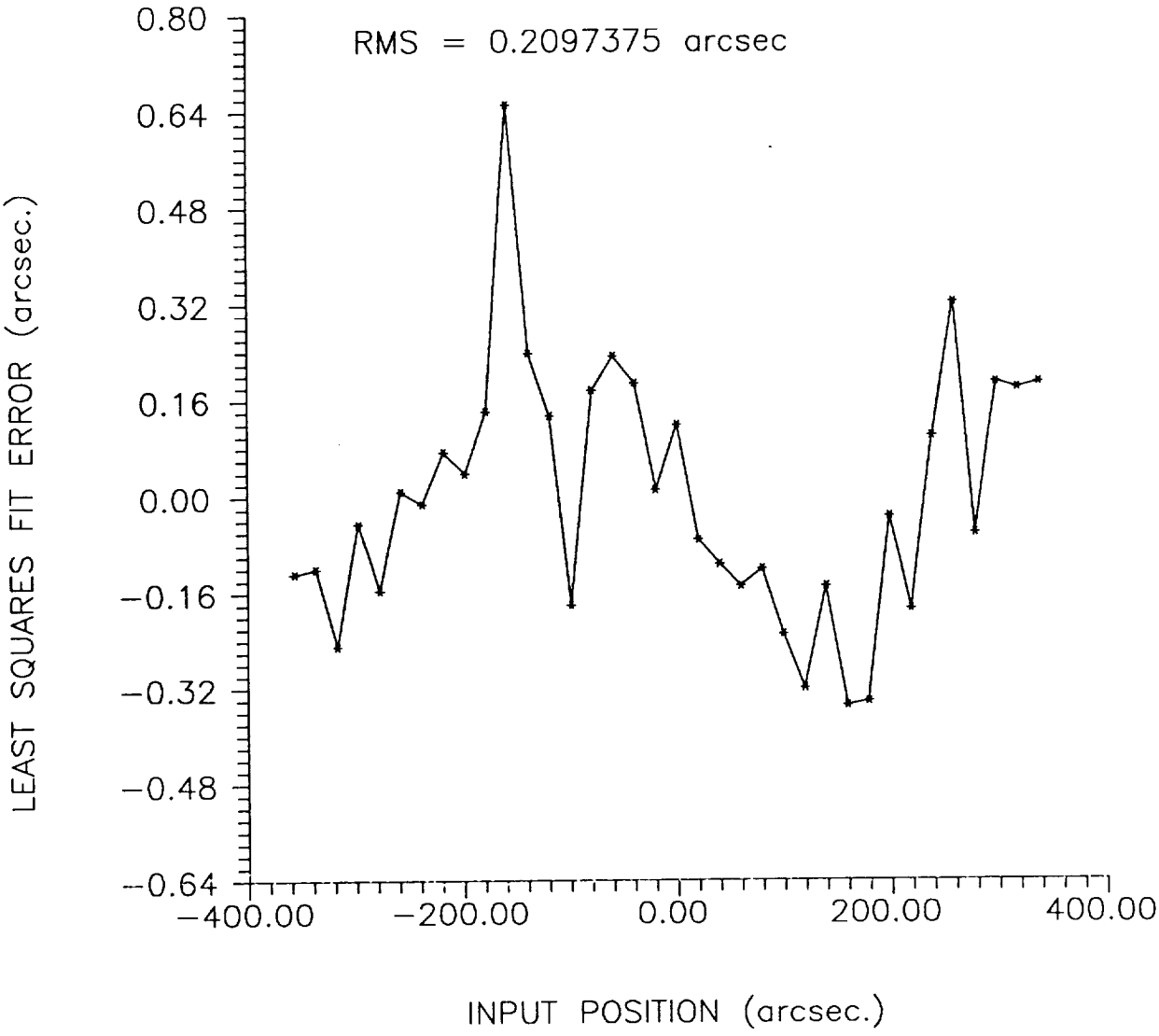

Figure 26: Y axis Third Order Approximation

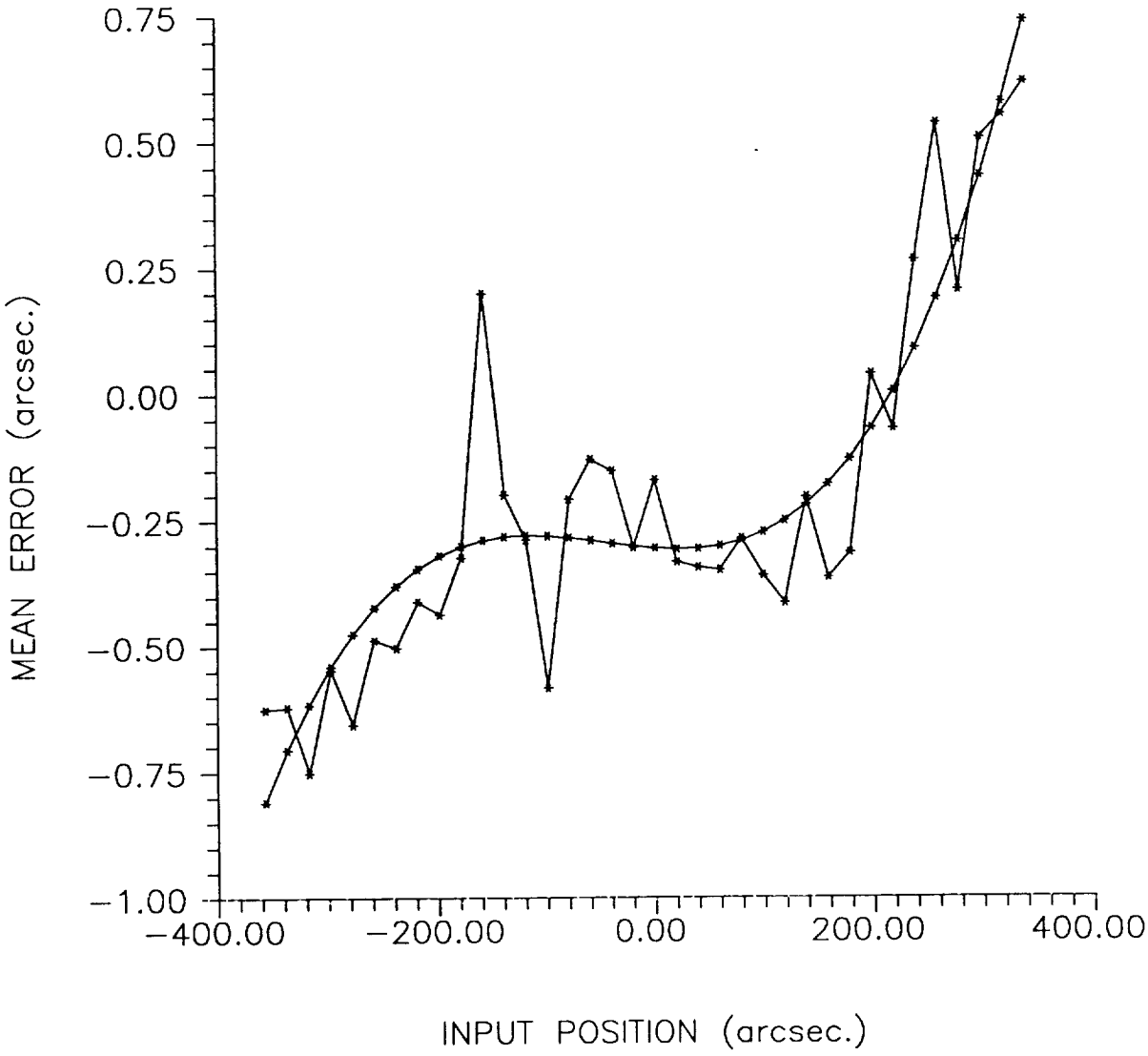

Figure 27: Y axis Third Order Approximation Error

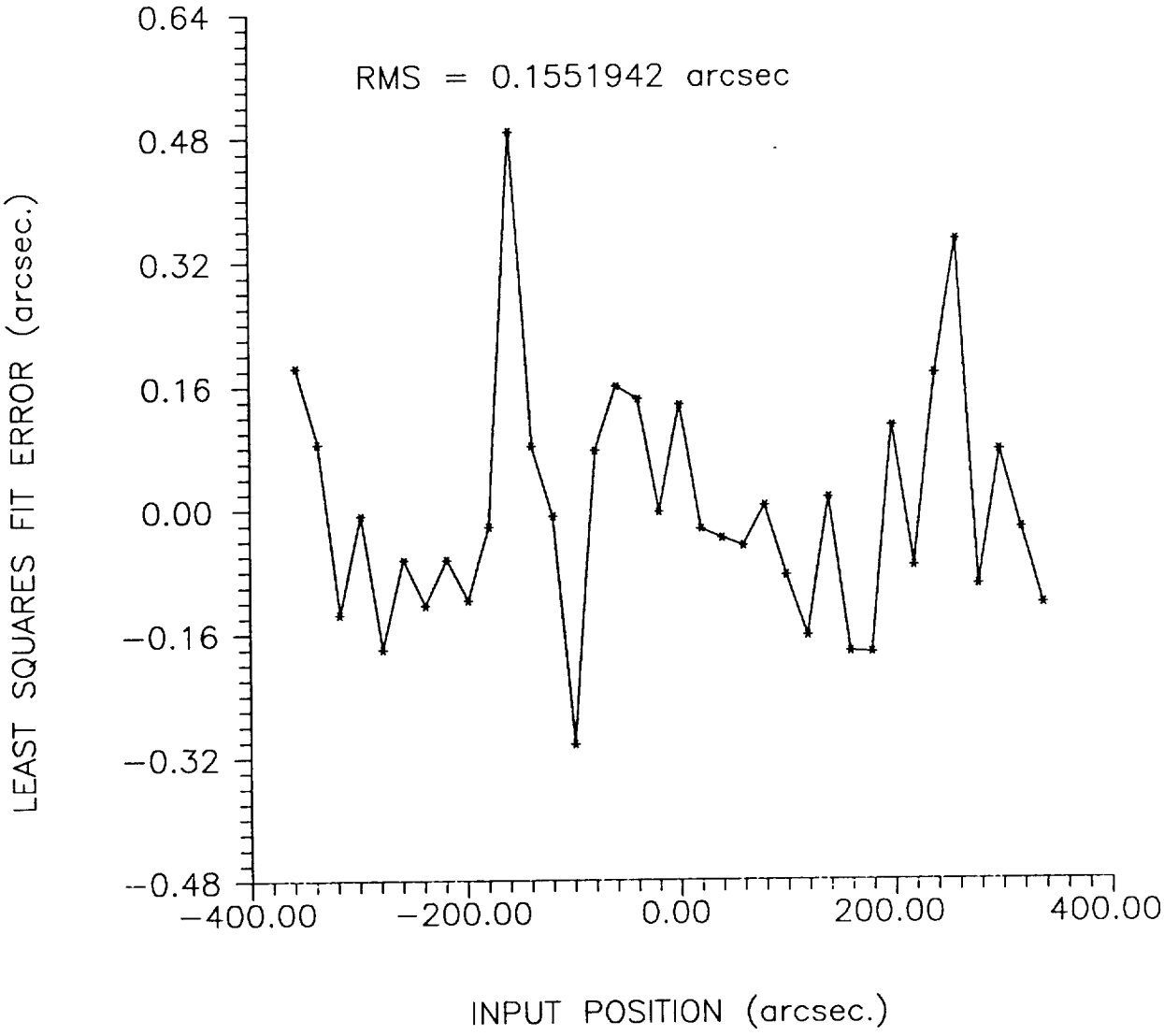

V. MODAL VIBRATION SENSOR USING THRESHOLD DETECTION

V.A. DESIGN

The design of the modal vibration sensor (MVS) for P/OF using threshold detection is based on the design of LOSS system to be implemented on HEIDi [6] and the LOSS system described in section IV. The design goal of the aspect system or LOSS for HEIDi was .2 arc sec. RMS absolute [7]. This accuracy has been demonstrated in laboratory tests [6].

An overview of the entire pointing control system (PCS) and solar aspect system (SAS) as developed at Auburn is shown in Figure 9. The system is composed of three main subsystems: the SAS, the PCS and the sunspot detector (SPD) system. The SAS uses four photo diode arrays (PDA's) to sense the solar image, as shown in Figure 10. The array outputs are video pulses which are serially clocked out of the arrays under the control of a microcomputer unit (MCU). The pulses from each PDA are amplified and converted to an envelope by a corresponding solar limb detector card (SLD). Each SLD card signals when the video output reaches a preset threshold level and from the timing of these signal, the MCU determines on which pixel the threshold was exceeded.

Since the solar image is very sharp due to focusing by a 5.2 m lens and associated optical filtering, the change in image intensity per pixel is greater than the variability of pixel response. This results in a limitation of crossing determination to $\pm$ .5 pixel. This figure results in an RMS error of .2 arc sec in a 5.2 m telescope. In a 32 m structure, the resulting RMS accuracy would be .0325 arc sec absolute without any other design changes. The HEIDi SAS currently is capable of operating at up to 250 hz.

The only design change required to implement a MVS is to replace the image generated by the sun to one generated by a white light source located adjacent to the detector array. This light is focused and projected to the back of the mask. Mirrors on the back of the mask refocus the light and return it to the detector arrays. Any movement of the mask in either axis is recorded as a change in the image center location. A schematic of the system is shown in Figure 28. Since an absolute measure of the vibrational angles are not required for modal control but only their frequency and amplitude, the only requirement of the system is that the light returned from the mask is sharply focused. This fact allows the usage of lenses in front of the detector array for image enhancement and ensures a sharply focused image.

Figure 28: Schematic of Moal Vibration Sensor (MVS)

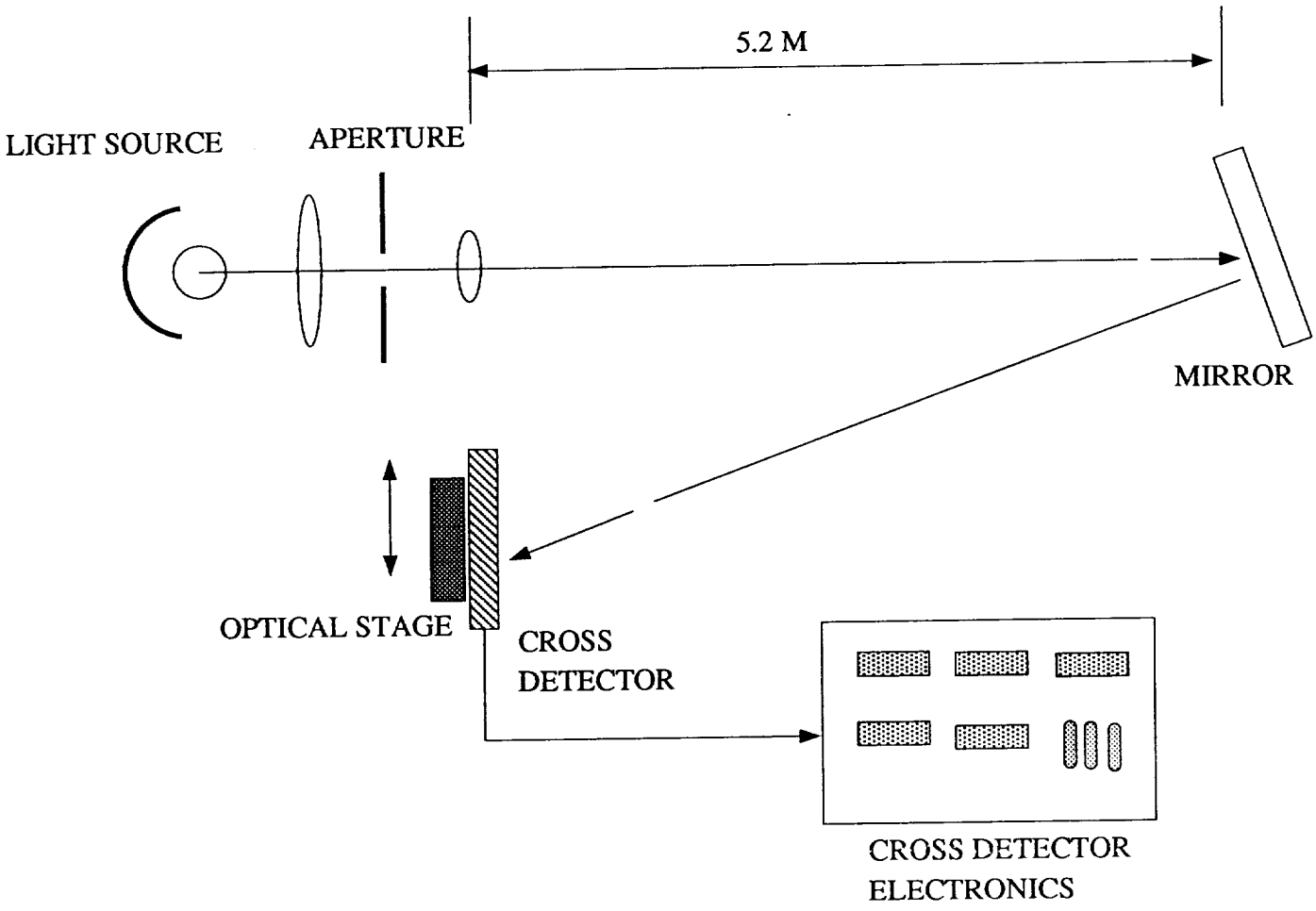

V.B. TESTING

The MVS system was tested in the laboratory using the experimental setup shown in Figure 11. The sensor was placed on an x - y translational stage and aligned with the beam produced by a projector placed next to it on the optical table. The optical path length of the test setup was 5.2 m from projector to mirror and from mirror to detector. The zero positions for both the x axis and y axis were set and rechecked before taking any data.

The calibration of each axis was performed independently of the other with the position of the other axis set to zero for the duration of the experiment. For the x axis position of the detector arrays was varied from this initial position in 20 arc second increments (500 μm steps). At each step, one thousand data points were taken by the system and averaged. This procedure was repeated 7 times to reduce offset errors caused by improper setting of the optical stage. The same procedure was repeated for the calibration of the y axis.

V.C. EXPERIMENTAL RESULTS

The results of the calibration of the x axis are shown in Figures 29 through 35. Figure 29 shows the mean error in the data for all runs. Without correction, the RMS error was .73 arc sec for a 5.2 m path length. A first order fit to the error is shown in Figure 30 and the error of that fit is given in Figure 31. The total RMS error of the first order fit was .28 arc sec for the 5.2 m path length. A second order fit is shown in Figure 32 and its error given in Figure 33. The total RMS error of the second order fit was .23 arc sec for the 5.2 m path length. A third order fit is shown in Figure 34 while the error of that fit is given in Figure 35. The total RMS error of the first order fit was .22 arc sec for the 5.2 m path length.

Similar results were obtained for the y axis and are shown in Figures 36 through 42. Once again the accuracy of the y axis is somewhat less than that of the x axis due to a defect in one of the photo diode arrays (Reticon RL1024 G). The x axis data is therefore more representative of the accuracy of the system and is approximately .2 arc sec RMS for a 5.2 m path length. The accuracy would scale to .0325 arc sec in the 32 m path length of P/OF.

Figure 29: X Axis; Total Mean Error vs. Position

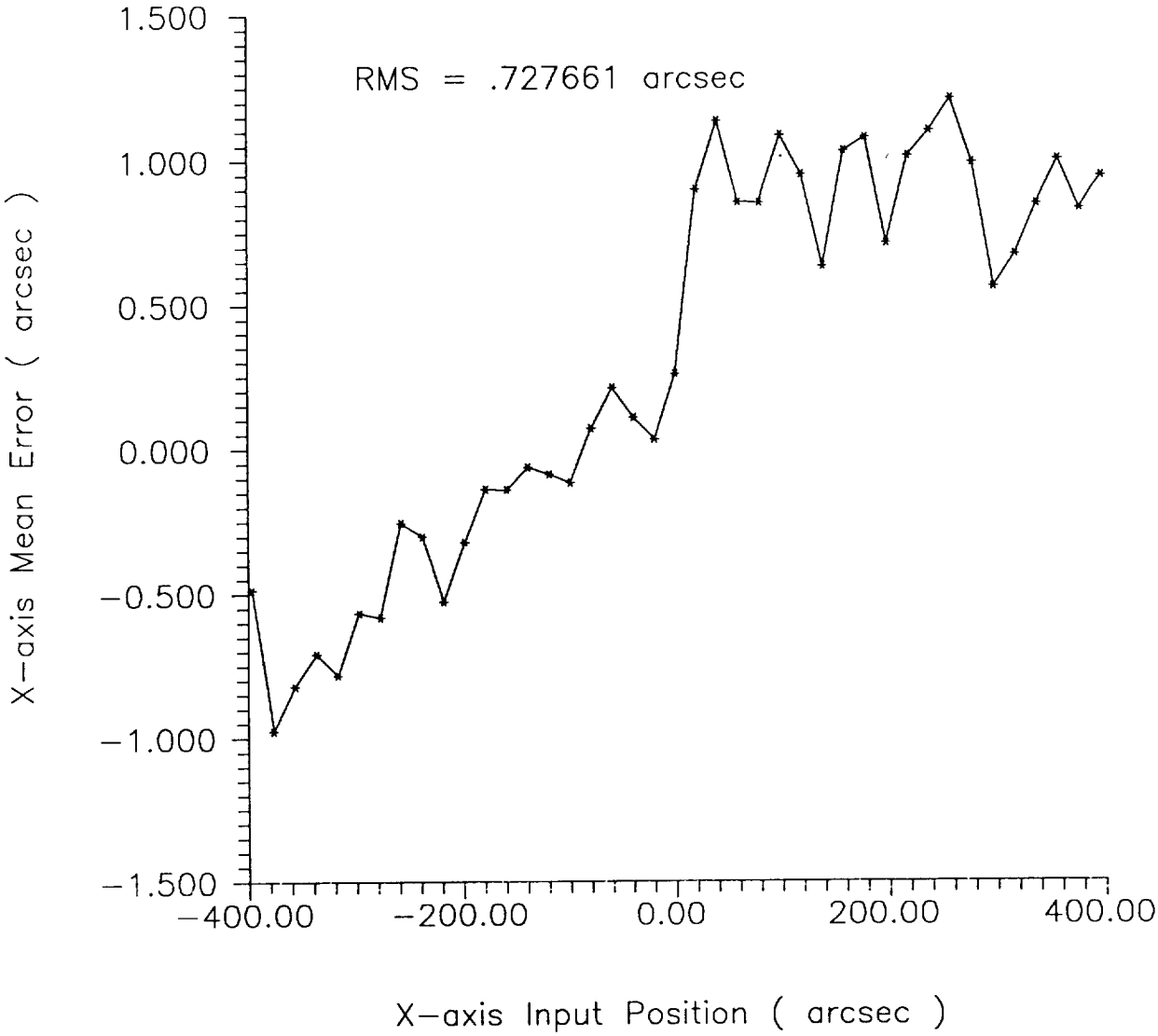

Figure 30: X Axis; First Order Approximation

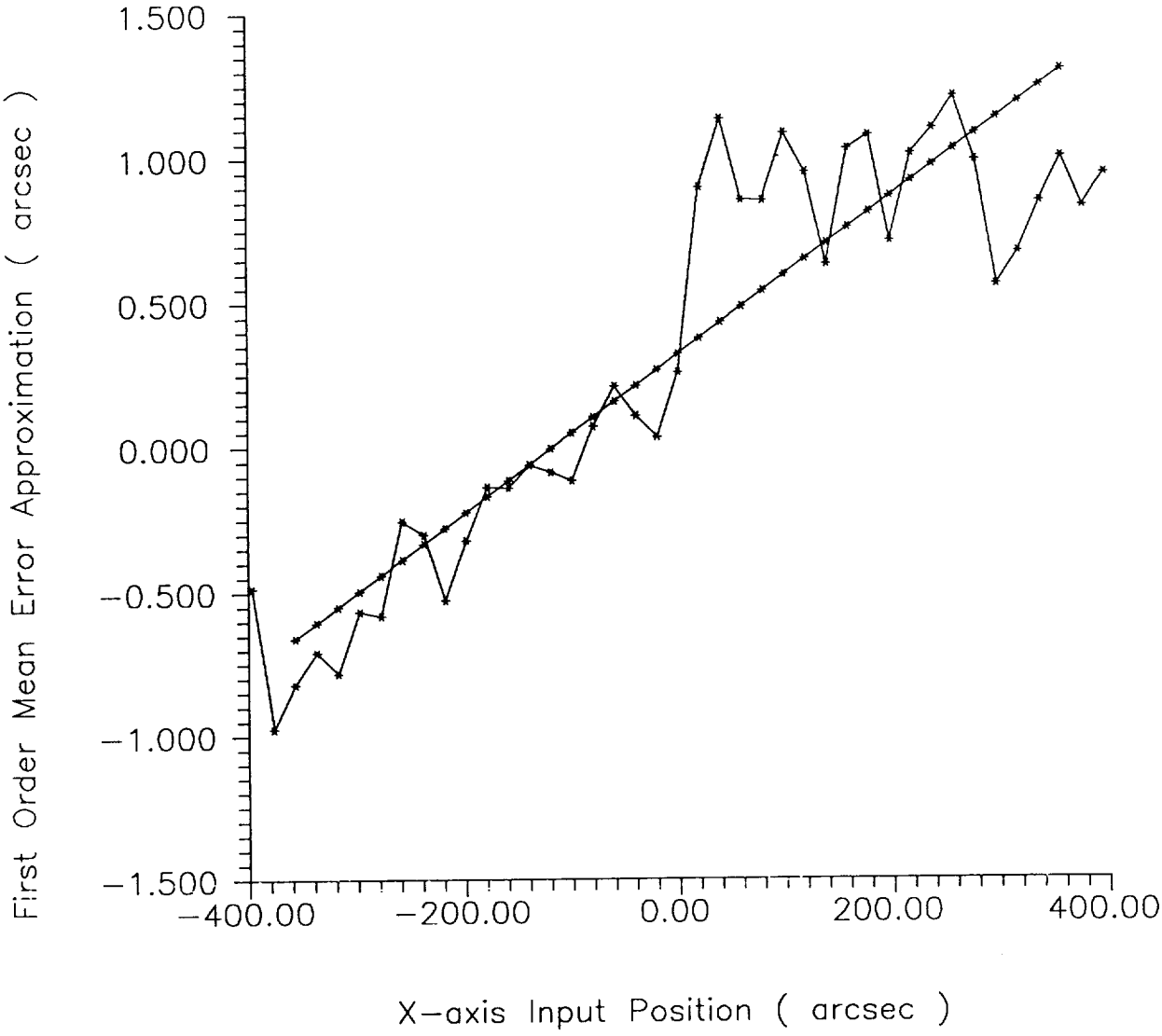

Figure 31: X Axis; First Order Approximation Error

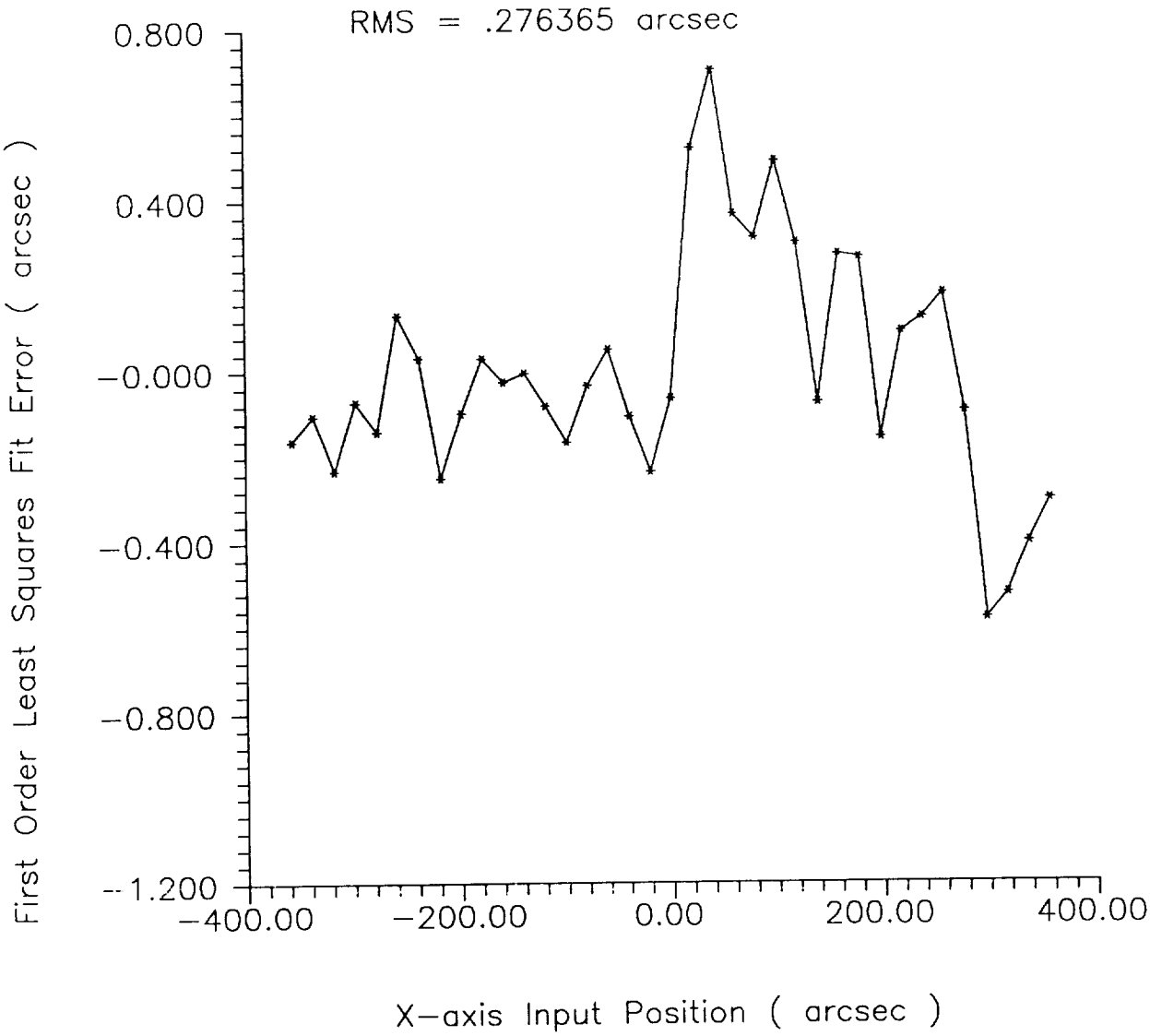

Figure 32: X Axis; Second Order Approximation

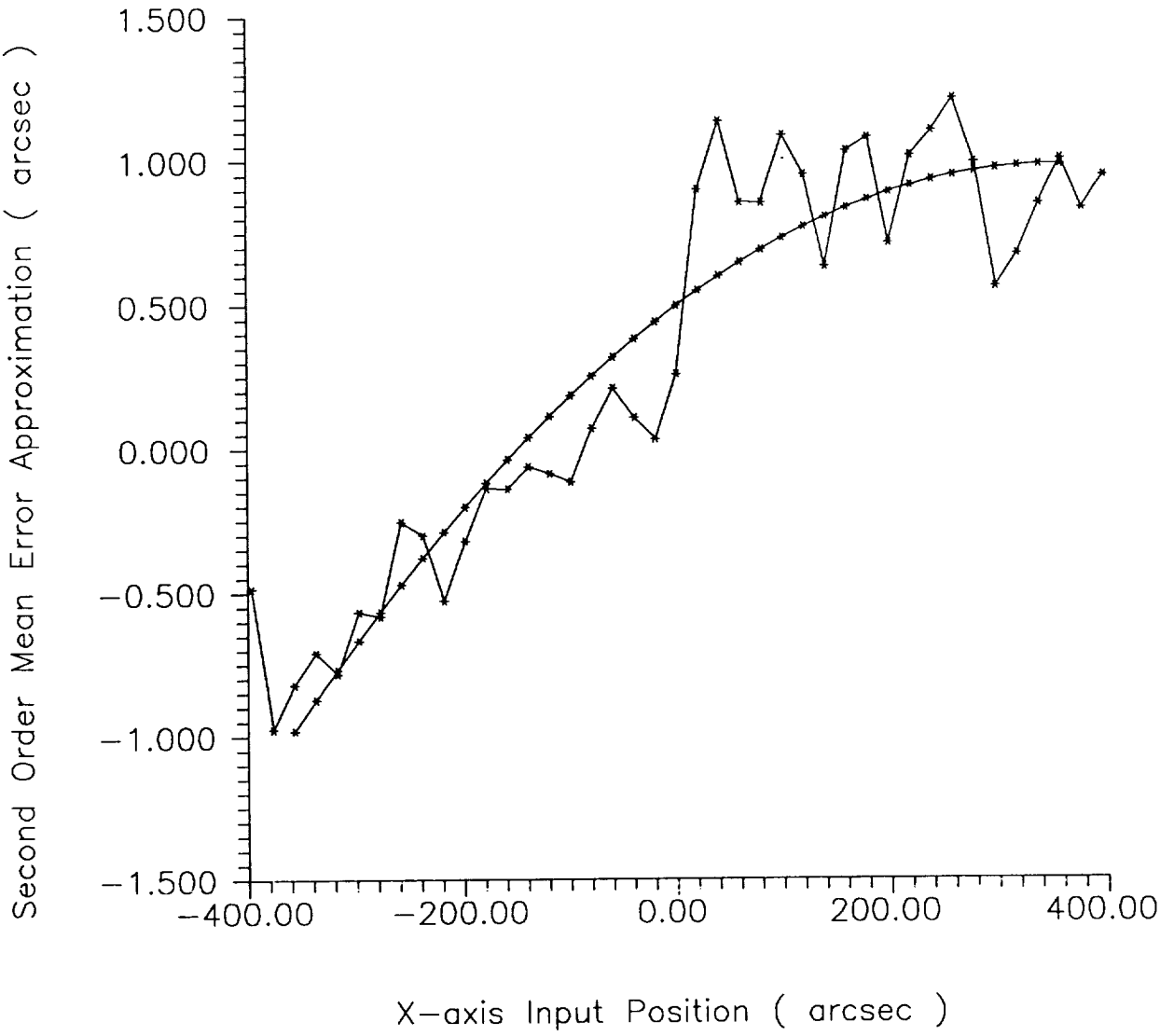

Figure 33: X Axis; Second Order Approximation Error

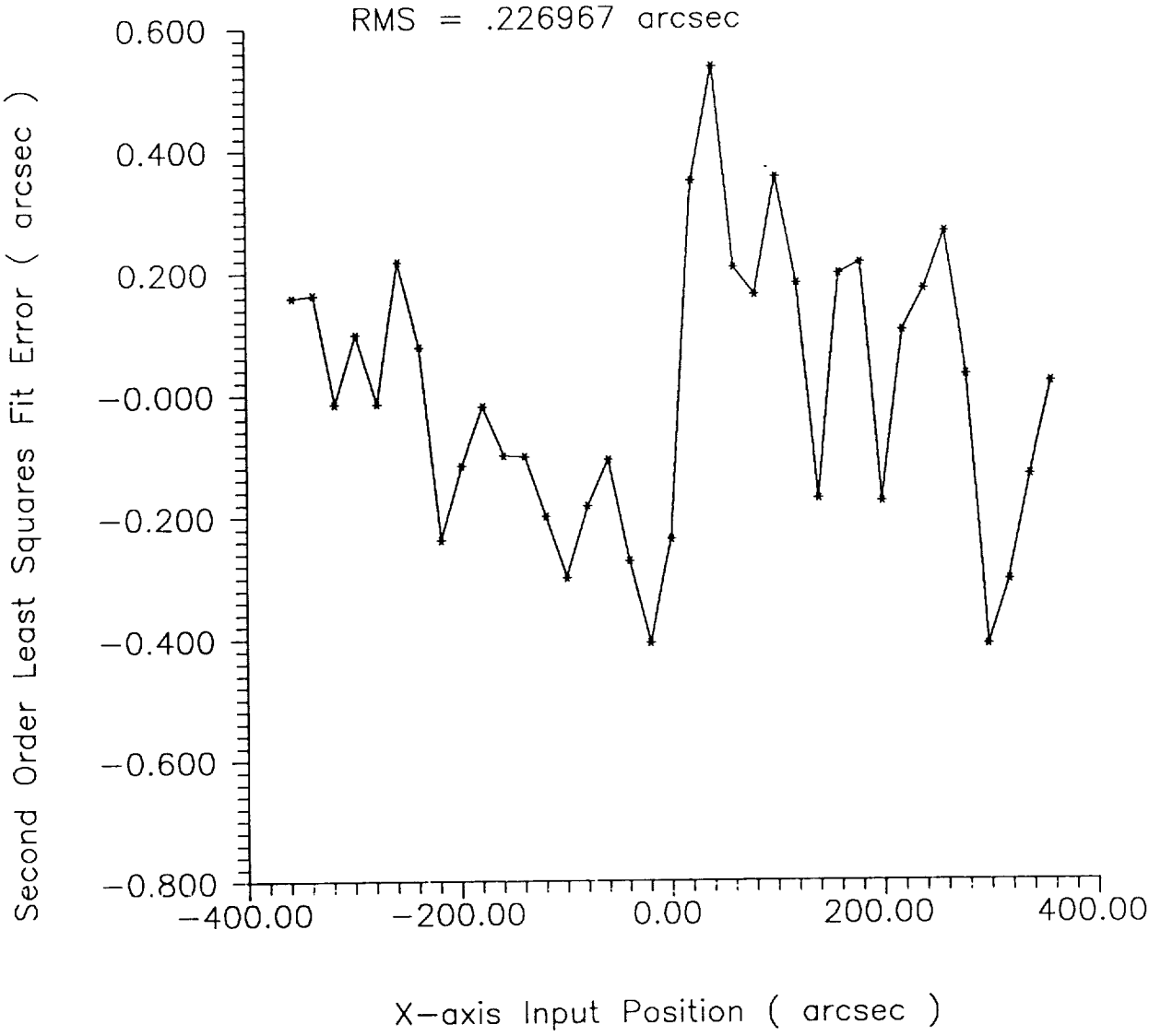

Figure 34: X Axis; Third Order Approximation

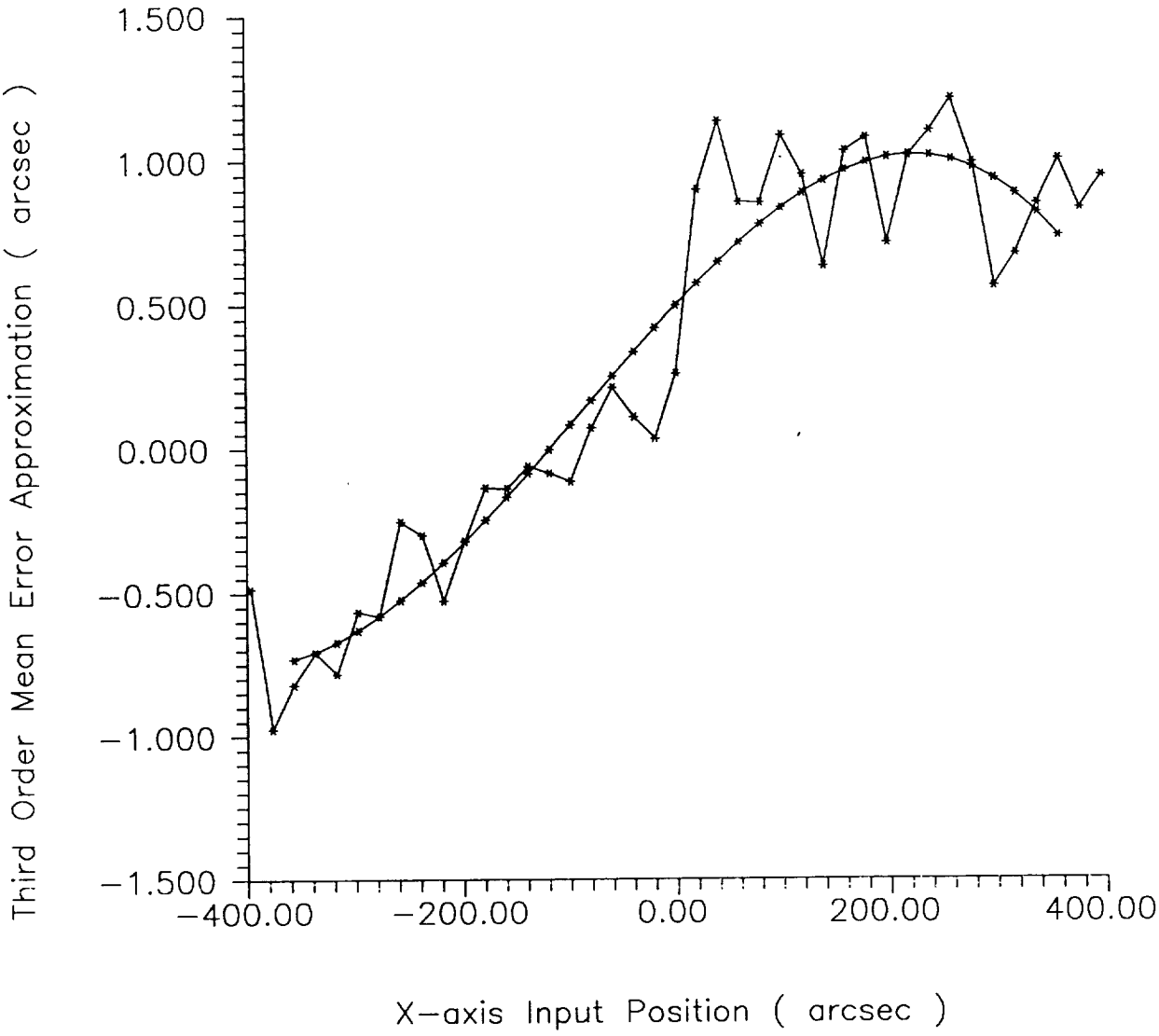

Figure 35: X Axis; Third Order Approximation Error

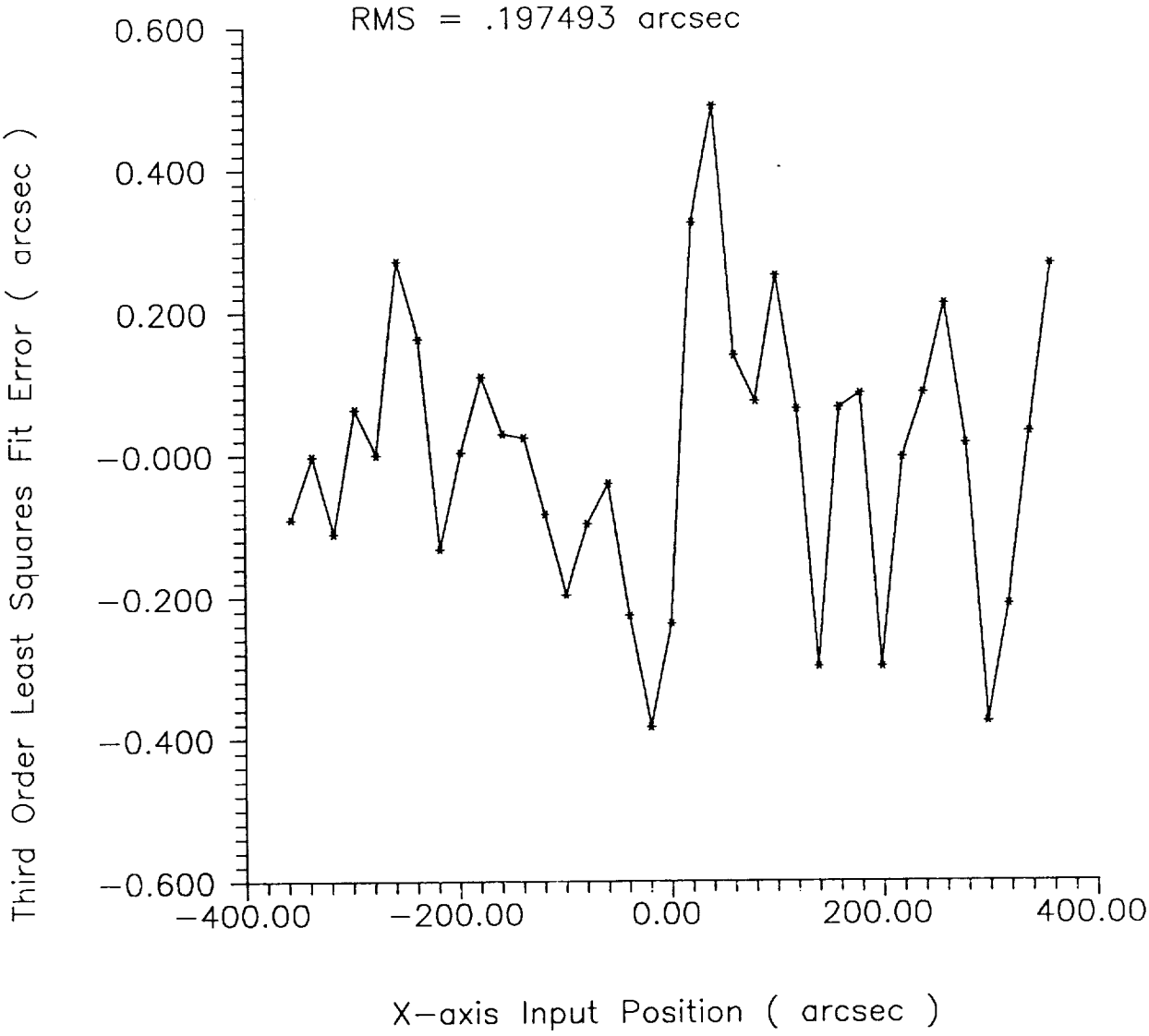

Figure 36: Y Axis; Total Mean Error vs. Position

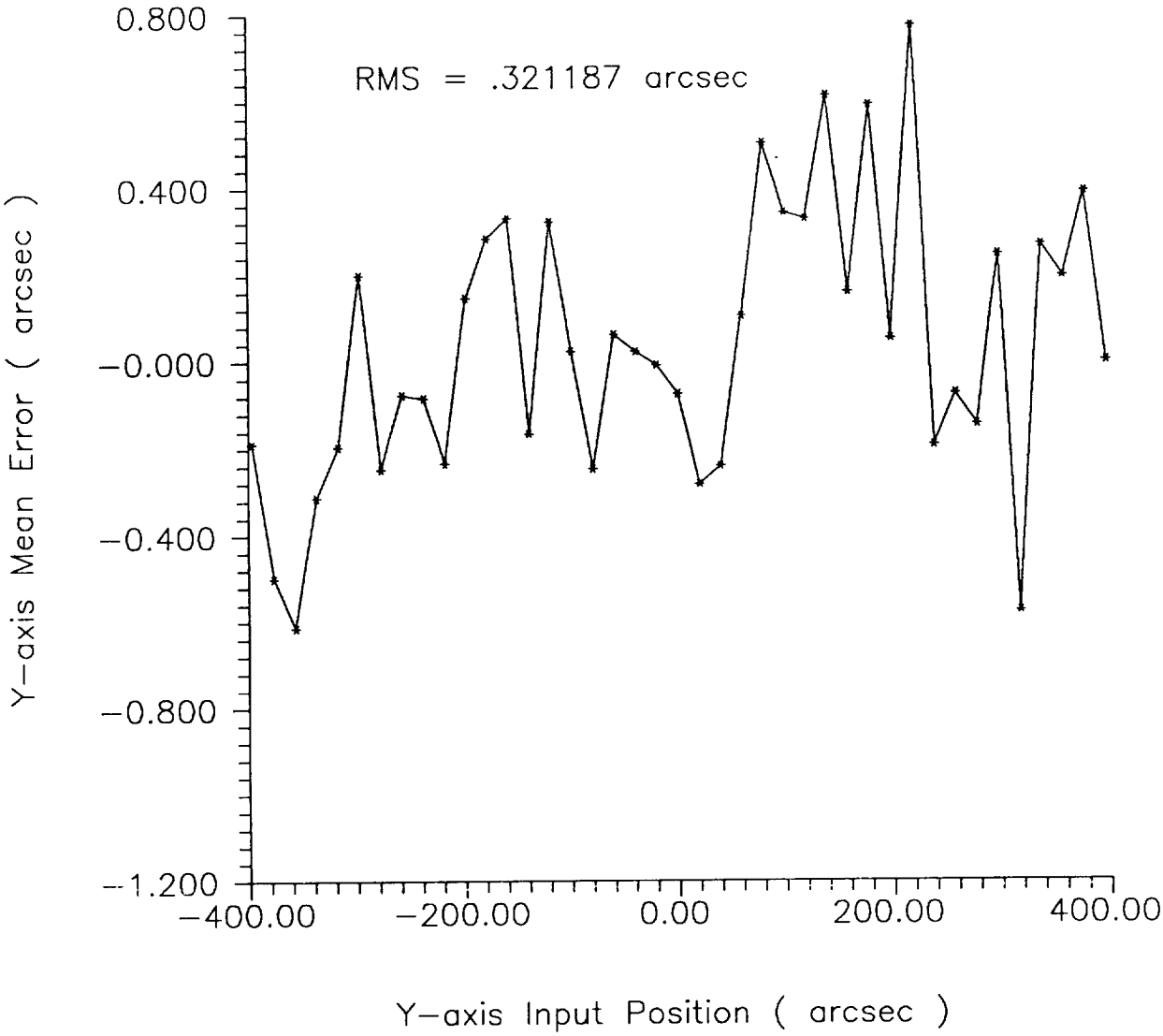

Figure 37: Y Axis; First Order Approximation

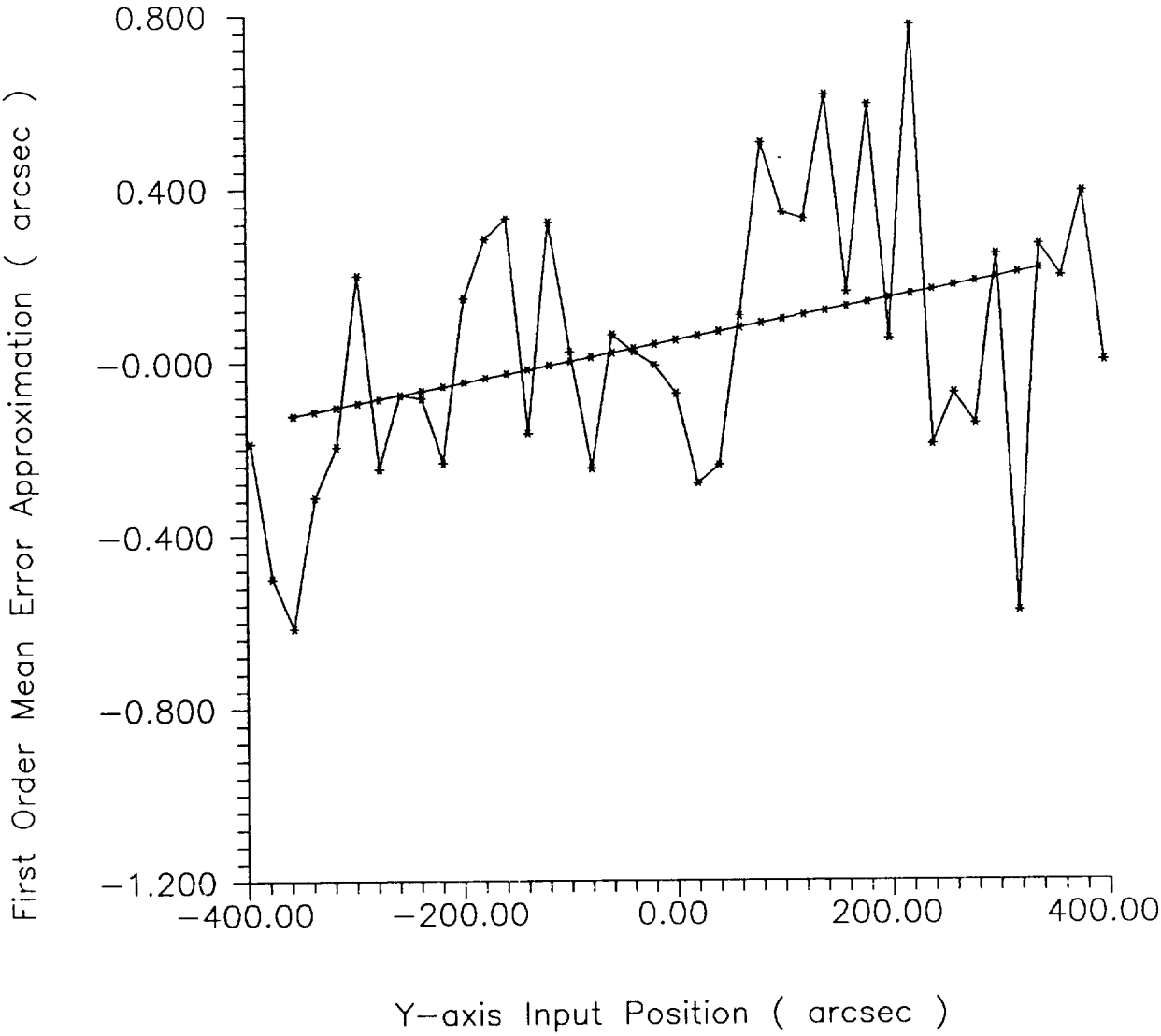

Figure 38: Y Axis; First Order Approximation Error

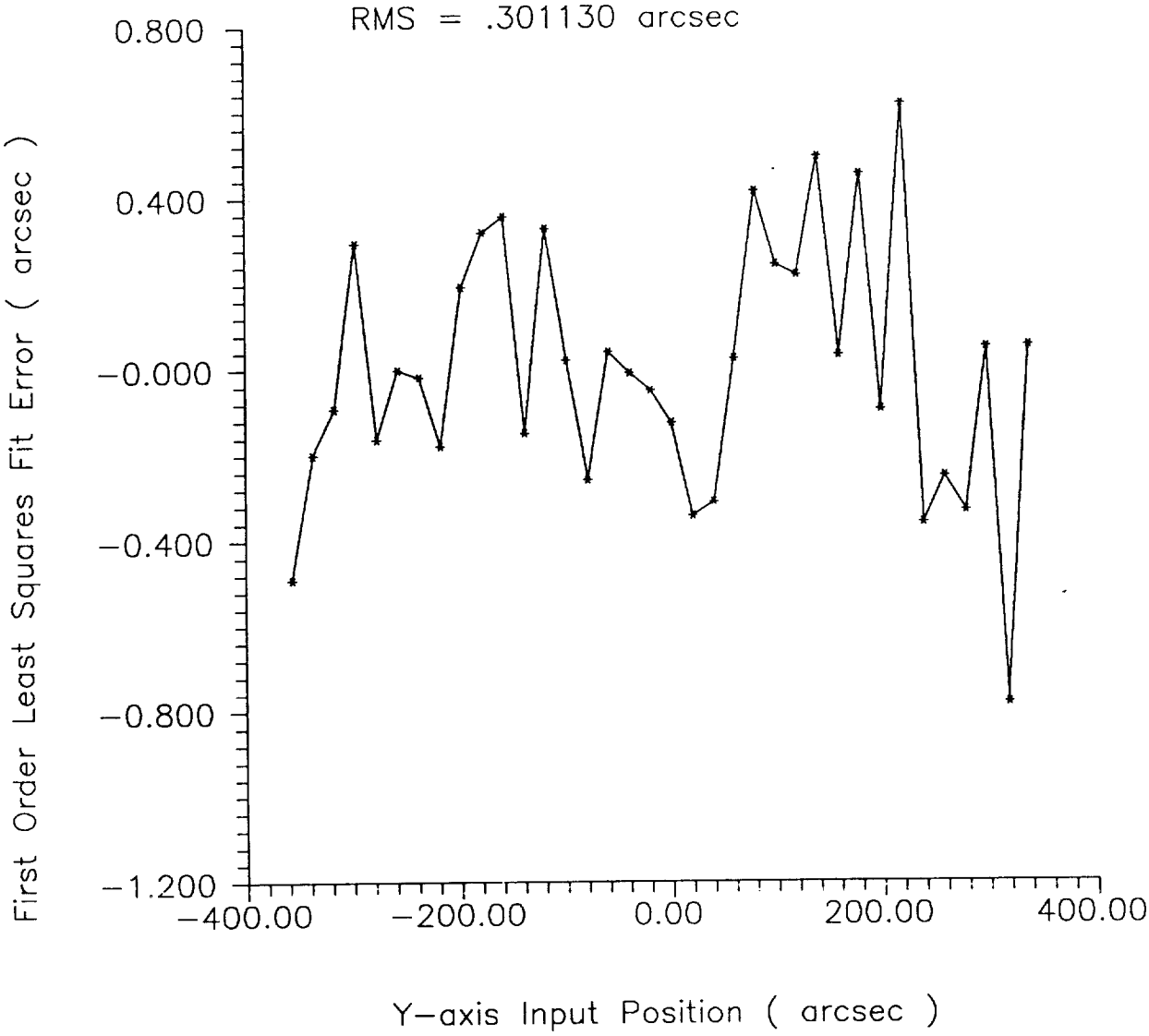

Figure 39: Y Axis; Second Order Approximation

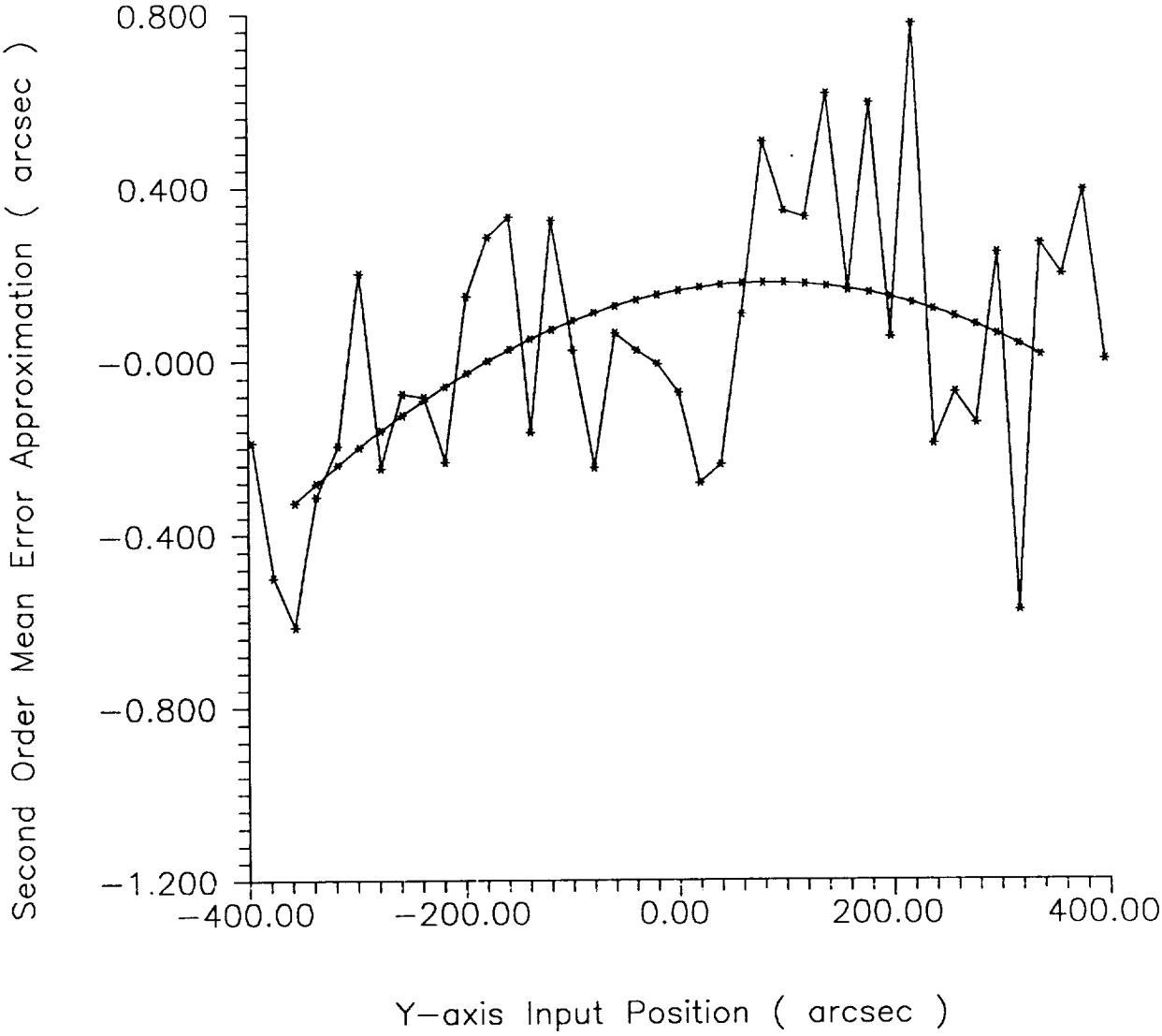

Figure 40: Y Axis; Second Order Approximation Error

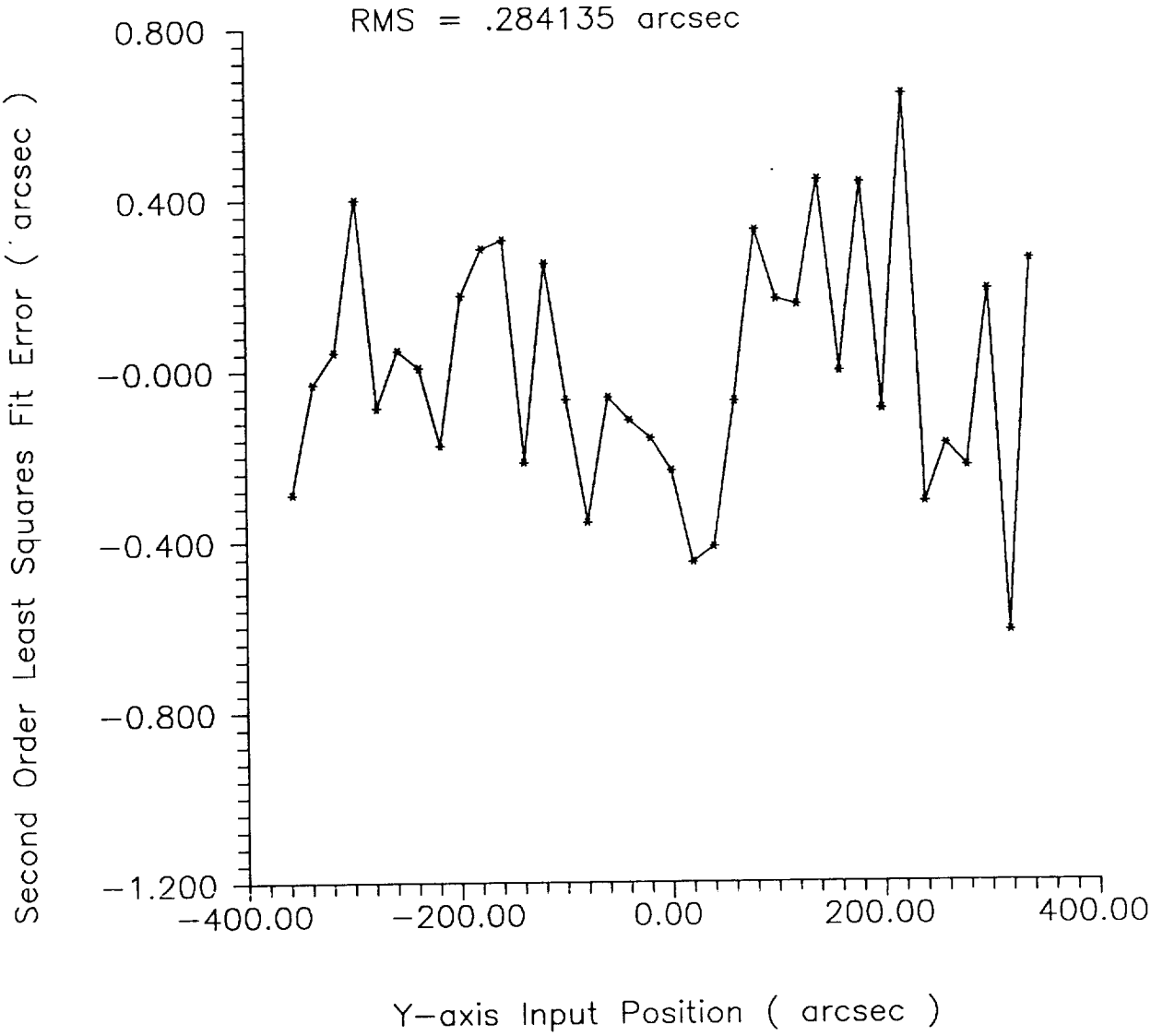

Figure 41: Y Axis; Third Order Approximation

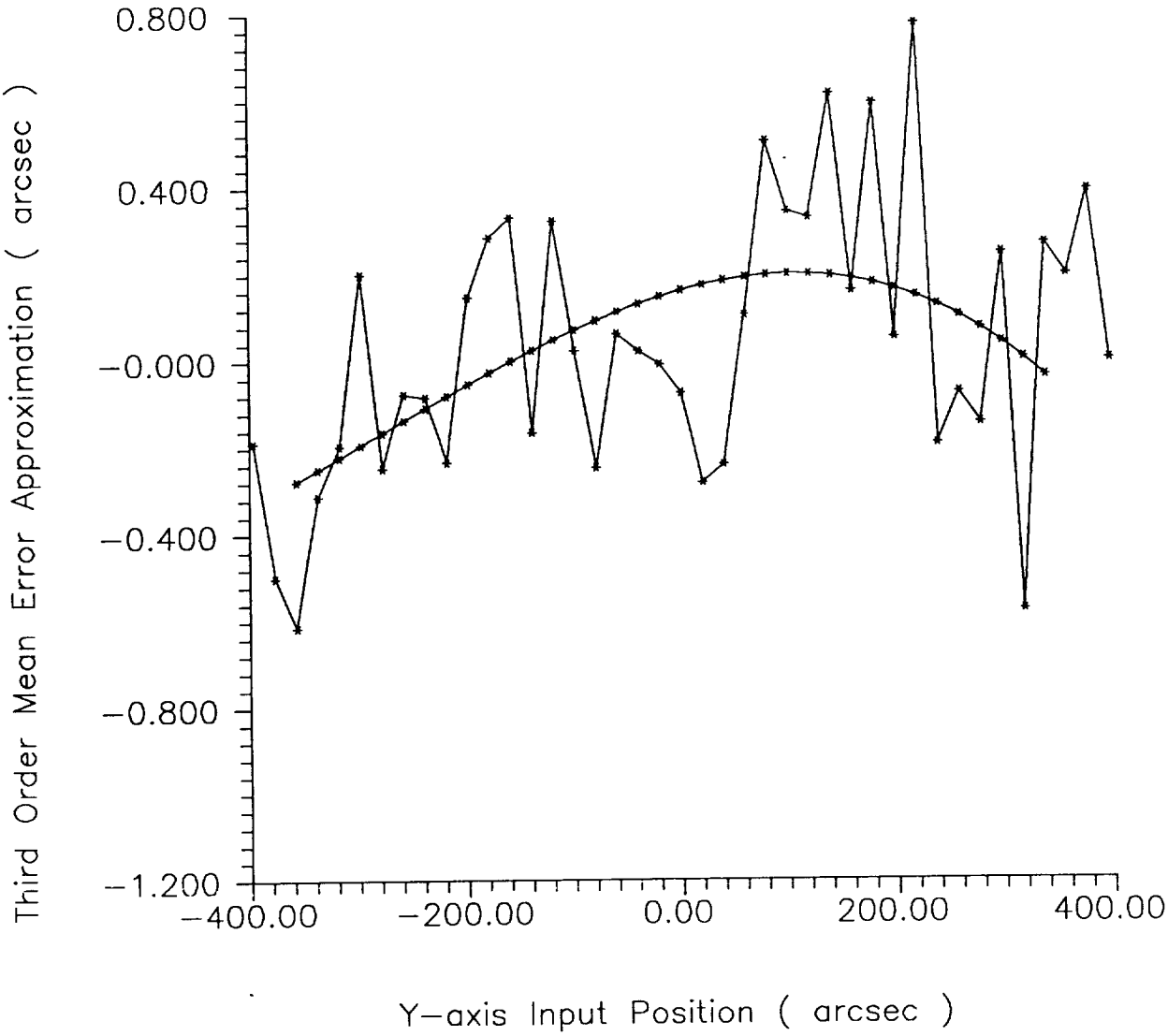

Figure 42: Y Axis; Third Order Approximation Error

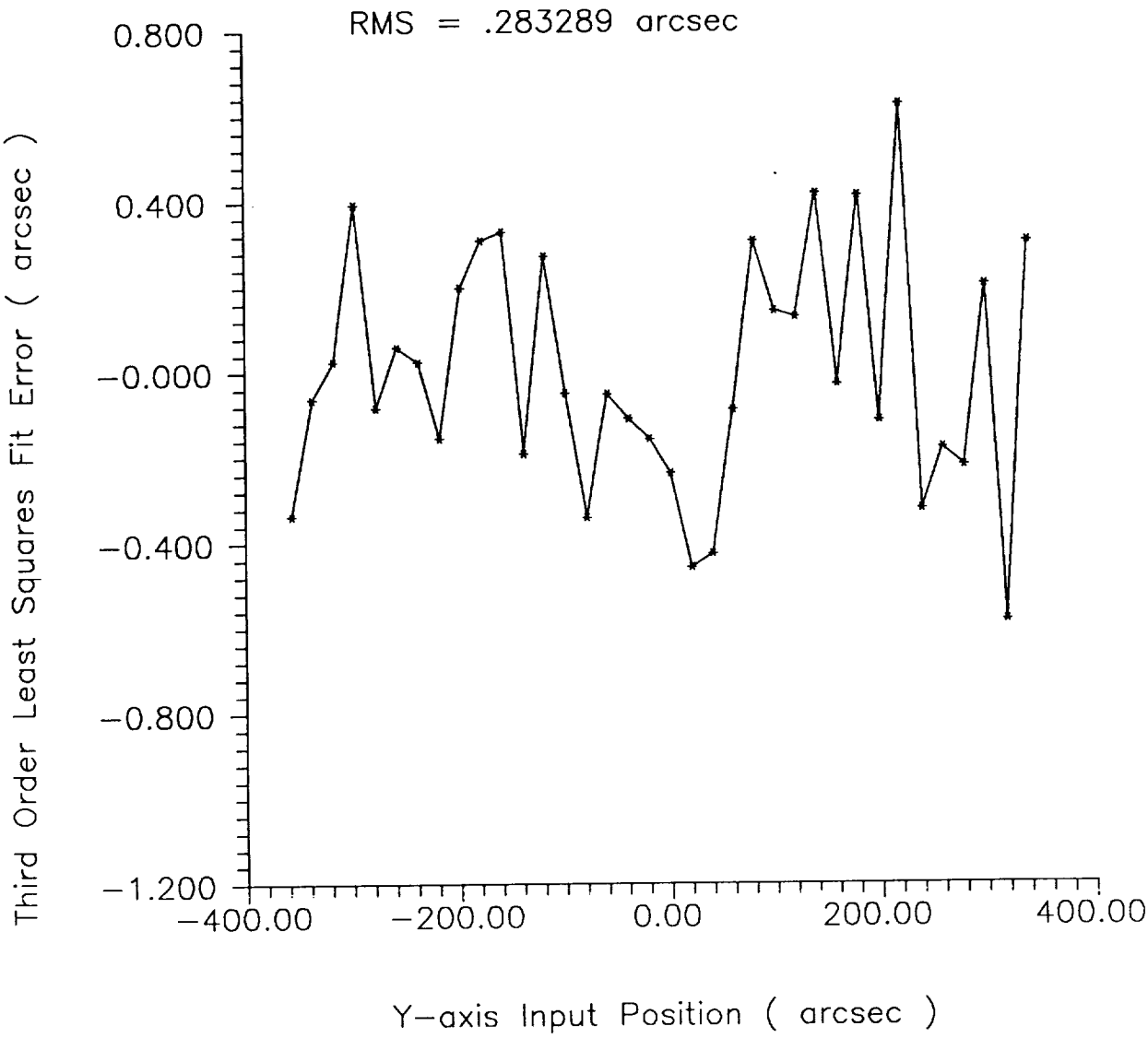

VI. CONCLUSIONS

Three laboratory prototypes have been developed and tested for the P/OF. The first was a LOSS based on measuring the slope of the solar image produced by a 5 mm pinhole in the mask of P/OF. The second prototype was based on the LOSS for HEIDi and used a sharp image of the sun and threshold detection to determine the solar center. The third prototype measured the modal vibrations internal to the system using a mirror, a projected light and the detection system based on threshold detection.

The first laboratory model of a LOSS developed and tested was based on using a pinhole in the mask of the P/OF and estimating sun center using the slopes of the resulting solar image. The hardware realization is relatively efficient and simple. Testing demonstrated that the sensor is able to provide a RMS accuracy 0.5 μm (.00032 arc seconds for a 32 m structure) in the measurement of pointing deflection. The results are limited strictly by environmental noises and experimental setup.

The second laboratory model of a LOSS developed and tested was based on using a sharply defined solar image and threshold techniques for edge detection. This technique has the advantages of even simpler hardware and software and as such can be operated at higher rates. Testing demonstrated a RMS accuracy of 5 μm (.0325 arc seconds in a 32 m structure) for measuring pointing deflection. However to ensure image sharpness per photo diode, a larger photo diode pixel would be required in the actual system reducing the accuracy to 8.33 μm (.0542 arc seconds). This detector system is based on the HEIDi aspect system developed at Auburn.

A third laboratory model of a MVS system was developed and tested based on the HEIDi aspect system with an internal white light source. The system as built demonstrated accuracies of approximately 5 μm (.0325 arc seconds in a 32 m structure). No modifications would be required that reduced the RMS accuracy of such a system in the full scale P/OF.

VII. REFERENCES

1. Greene, M. "Pinhole/Coronograph Pointing Control System Integration and Noise Reduction Analysis," Final Report, NASA Contract # NAS 8 -34529, 1981

2 Greene, M., "Active Modal Damping of the Pinhole/Occulter Facility", Adv. Eng. Software: 7; 88-90,1985

3. Greene, M.,"Robustness of Active Model Damping of Large Flexible Structures", Int. J. Control: 46;1009-1018,1987

4. Greene, M. & Tan, H., "Solar Tracking: Design and Simulation", Proc 20th SSST; pp 208 - 211, 1988

5. Greene, M. & Tan, H., "An Optical Line of Sight Sensor for the Pinhole Facility," Proc 21st SSST; pp 536-540, 1989

6. Greene, M. & Divelbiss, A., "A High Energy Imaging Device (HEIDi) on a Balloon (Aspect System)," Phase B Report, NASA Contract # NAS 5 - 30759, 1990

7.Divelbiss, A., Greene, M., & Rich, A. "An Optical Aspect Sensor for the Gamma Ray Imaging Device," Proc 22nd SSST; pp 344 - 348, 1990

8.Description and Requirement Document for the HEIDi (HIgh Energy Imaging Device) Mission, Preliminary, Nov 14, 1990